

1 SEARCH FOR PRODUCTION OF A HIGGS BOSON AND A SINGLE TOP
2 QUARK IN MULTILEPTON FINAL STATES IN pp COLLISIONS AT $\sqrt{s} = 13$
3 TeV.

4 by

5 Jose Andres Monroy Monta  ez

A DISSERTATION

7 Presented to the Faculty of

8 The Graduate College at the University of Nebraska

9 In Partial Fulfilment of Requirements

10 For the Degree of Doctor of Philosophy

11 Major: Physics and Astronomy

12 Under the Supervision of Kenneth Bloom and Aaron Dominguez

13 Lincoln, Nebraska

14 July, 2018

15 SEARCH FOR PRODUCTION OF A HIGGS BOSON AND A SINGLE TOP
16 QUARK IN MULTILEPTON FINAL STATES IN pp COLLISIONS AT $\sqrt{s} = 13$
17 TeV.

18 Jose Andres Monroy Montañez, Ph.D.

19 University of Nebraska, 2018

20 Adviser: Kenneth Bloom and Aaron Dominguez

²¹ Table of Contents

²²	Table of Contents	iii
²³	List of Figures	vi
²⁴	List of Tables	viii
²⁵	1 INTRODUCTION	1
²⁶	2 Theoretical approach	2
²⁷	2.1 Introduction	2
²⁸	2.2 Standard model of particle physics	5
²⁹	2.2.1 Fermions	7
³⁰	2.2.1.1 Leptons	8
³¹	2.2.1.2 Quarks	10
³²	2.2.2 Fundamental interactions	14
³³	2.2.3 Gauge Bosons	19
³⁴	2.3 Electroweak unification and the Higgs mechanism	21
³⁵	2.3.1 Spontaneous symmetry breaking	29
³⁶	2.3.2 Higgs mechanism	33
³⁷	2.3.3 Masses of the gauge bosons	35

38	2.3.4	Masses of the fermions	36
39	2.3.5	The Higgs field	37
40	2.3.6	Higgs boson production mechanisms at LHC.	38
41	2.3.7	Higgs decay channels	42
42	2.4	Associated Production of Higgs Boson and Single Top Quark.	43
43	2.5	The CP-mixing in tH processes	48
44	3	The CMS experiment at the LHC	52
45	3.1	Introduction	52
46	3.2	The LHC	53
47	3.3	The CMS experiment	57
48	4	Search for production of a Higgs boson and a single top quark in multilepton final states in pp collisions at $\sqrt{s} = 13$ TeV	59
50	4.1	Introduction	59
51	4.2	Data and MC Samples	61
52	4.2.1	Full 2016 dataset and MC samples	61
53	4.2.2	Triggers	64
54	4.2.2.1	Trigger efficiency scale factors	64
55	4.3	Object Identification and event selection	65
56	4.3.1	Jets and b tagging	65
57	4.3.2	Lepton selection	66
58	4.3.3	Lepton selection efficiency	67
59	4.4	Background predictions	68
60	4.5	Signal discrimination	69
61	4.5.1	Classifiers response	73
62	4.6	Additional discriminating variables	76

63	5 The CMS forward pixel detector	79
64	5.0.1 The phase 1 FPix upgrade	79
65	5.0.2 FPix module production line	79
66	5.0.3 The Gluing stage	79
67	5.0.4 The Encapsulation stage	79
68	5.0.5 The FPix module production yields	79
69	Bibliography	79
70	References	80

⁷¹ List of Figures

72	1.1	^{14}N neutron capture in a PECVD polymerized pyridine film. The Q-value of this reaction is 626 keV. Taken from [22]	1
74	2.1	Standard model of particle physics.	6
75	2.2	WI transformations between quarks	13
76	2.3	Fundamental interactions in nature.	14
77	2.4	SM interactions diagrams	15
78	2.5	Neutral current processes	22
79	2.6	Spontaneous symmetry breaking mechanism	29
80	2.7	SSB Potential form	30
81	2.8	Potential for complex scalar field	31
82	2.9	SSB mechanism for complex scalar field	32
83	2.10	Proton-Proton collision	39
84	2.11	Higgs production mechanism Feynman diagrams	40
85	2.12	Higgs production cross section and decay branching ratios	41
86	2.13	Associated Higgs production mechanism Feynman diagrams	43
87	2.14	Cross section for tHq process as a function of C_t	46
88	2.15	Cross section for tHW process as a function of κ_{Htt}	46
89	2.16	NLO cross section for tX_0 and $t\bar{t}X_0$	50

90	2.17 NLO cross section for tWX_0 , $t\bar{t}X_0$ and $tWX_0 + t\bar{t}X_0 + \text{interference}$. . .	51
91	3.1 ref. C.Lefevre, “The CERN accelerator complex,” (2008). CERN-DI-	
92	0812015.	54
93	3.2 ref. J.-L. Caron , “Layout of the LEP tunnel including future LHC in-	
94	frastructures.. L’ensemble du tunnel LEP avec les futures infrastructures	
95	LHC.”, https://cds.cern.ch/record/841542 (Nov, 1993). AC Collection.	
96	Legacy of AC. Pictures from 1992 to 2002..	55
97	3.3 ref. ACTeam, “Diagram of an LHC dipole magnet. Schéma d’un aimant	
98	dipôle du LHC,” (1999). CERN-DI-9906025.	56
99	3.4 ref: CMS Collaboration, “Detector Drawings”, CMS-PHO-GEN-2012-002,	
100	http://cds.cern.ch/record/1433717 , 2012.	58
101	4.1 The two leading-order diagrams of tHq production.	60
102	4.2 Input variables to the BDT for signal discrimination normalized.	70
103	4.3 Input variables to the BDT for signal discrimination not normalized. . .	72
104	4.4 BDT inputs as seen by TMVA against $t\bar{t}$	73
105	4.5 BDT inputs as seen by TMVA against $t\bar{t}\bar{V}$	74
106	4.6 Correlation matrices for the input variables in the TMVA.	75
107	4.7 MVA classifiers performance.	75
108	4.8 Additional discriminating variables distributions.	77

¹⁰⁹ List of Tables

110	2.1	Fermions of the SM.	7
111	2.2	Leptons properties.	10
112	2.3	Quarks properties.	10
113	2.4	Fermion weak isospin and weak hypercharge multiplets.	12
114	2.5	Fundamental interactions features.	16
115	2.6	SM gauge bosons.	21
116	2.7	Higgs boson properties.	38
117	2.8	Predicted branching ratios for a SM Higgs boson with $m_H = 125 \text{ GeV}/c^2$	42
118	2.9	Predicted SM cross sections for tH production at $\sqrt{s} = 13 \text{ TeV}$	44
119	2.10	Predicted enhancement of the tHq and tHW cross sections at LHC	47
120	4.1	Signal samples and their cross section and branching fraction.	61
121	4.2	κ_V and κ_t combinations.	62
122	4.3	List of background samples used in this analysis (CMSSW 80X).	63
123	4.4	Leading-order $t\bar{t}W$ and $t\bar{t}Z$ samples used in the signal BDT training.	63
124	4.5	Table of high-level triggers that we consider in the analysis.	64
125	4.6	Trigger efficiency scale factors and associated uncertainties.	65
126	4.7	Requirements on each of the three muon selections.	66
127	4.8	Criteria for each of the three electron selections.	67

128	4.9 MVA input discriminating variables	71
129	4.10 TMVA input variables ranking for BDTA_GRAD method	76
130	4.11 TMVA configuration used in the BDT training.	76
131	4.12 ROC-integral for all the testing cases.	78

¹³² Chapter 1

¹³³ INTRODUCTION

Figure 1.1: ^{14}N neutron capture in a PECVD polymerized pyridine film. The Q-value of this reaction is 626 keV. Taken from [22]

¹³⁴ Chapter 2

¹³⁵ Theoretical approach

¹³⁶ 2.1 Introduction

¹³⁷ The physical description of the universe is a challenge that physicists have faced by
¹³⁸ making theories that refine existing principles and proposing new ones in an attempt
¹³⁹ to embrace emerging facts and phenomena. By early 1800's, there were separate the-
¹⁴⁰ ories describing electric and magnetic phenomena, gravitational force and light. The
¹⁴¹ invention of the electric battery by Alessandro Volta in 1800, the discovery of the
¹⁴² magnetic effects of the electric current by Oersted and Ampere (1820), and the gen-
¹⁴³ eration of electric current using changing magnetic fields by Faraday (1831) represent
¹⁴⁴ the first steps in the way to create a unified theory of electromagnetism [1].

¹⁴⁵

¹⁴⁶ The unification was carried out by James Clerk Maxwell who was able to merge elec-
¹⁴⁷ tricity and magnetism in a set of 20 equations known as "general equations of the
¹⁴⁸ electromagnetic field," relating the observables that describe the experimental laws of
¹⁴⁹ the electromagnetism. By combining these equations, Maxwell found a wave equation
¹⁵⁰ and propose the existence of the "electromagnetic waves." The predicted propagation

151 speed of the electromagnetic waves turned out to be the same as the speed of light,
152 therefore, the natural conclusion was that light is an electromagnetic wave [4]. By
153 1900, waves were considered a perturbation of a material medium which in the case
154 of the electromagnetic waves was identified as the “*Luminiferous Ether*”.

155

156 By 1900, Max Planck came out with the idea that radiation is quantized [5] and Albert
157 Einstein in 1905 made use of that hypothesis to propose the existence of the light
158 quantum, the “*photon*”, in order to explain the photoelectric effect [6]. The well-
159 known quantum revolution in physics started and the idea of particle-wave duality
160 of photons as a natural behavior was developed and later extended to electrons and
161 to all kind of particles in nature. The development of a quantum theory allowed to
162 predict a set of non-common sense effects like the quantum tunneling and quantum
163 entanglement, however, quantum theory was separated from the recently unified elec-
164 tromagnetism.

165

166 In 1905, Einstein also published two more papers; one aimed to describe his statistical
167 molecular theory of liquids and how it can be used to describe Brownian motion [7].
168 At that time the existence of the atoms and molecules were not fully demonstrated
169 but Einstein’s theory provided an explanation as well as predictions based on the
170 their existence. Jean Perrin in 1908 conducted experiments that confirmed Einstein’s
171 predictions. The other paper described the relationship between space and time [8],
172 unifying the notion of space and time into one entity known as “*spacetime*” that treats
173 space and time at the same level and then discards the absoluteness of time. The
174 new theory known as special relativity, supersedes the Galilean relativity principle
175 and postulates exceptional effects like the time dilation, length contraction and mass-

176 energy equivalence through the most famous formula in physics [9]

$$E = mc^2. \quad (2.1)$$

177 Generalization of the special relativity was presented in 1916 and includes a gener-
178 alization of Newton's law of universal gravitation, becoming a unified description of
179 gravity as a geometric property of space and time. Einstein's predictions include the
180 existence of black holes and the recently observed "*gravitational waves*" [10].

181 At the end of 1940s Julian Schwinger [11] and Richard P. Feynman [12], based in
182 the work of Sin-Itiro Tomonaga [13], developed an electromagnetic theory consistent
183 with special relativity and quantum mechanics that describes how matter and light
184 interact; so-called "quantum eletrodynamics" (QED) had born.

185

186 QED has become the guide in the development of theories that describe the universe.
187 It was the first example of a quantum field theory (QFT), which is the theoretical
188 framework for building quantum mechanical models that describes particles and their
189 interactions. QFT is composed of a set of mathematical tools that combines classical
190 fields, special relativity, and quantum mechanics while keeping the quantum point
191 particles and locality ideas. This chapter gives an overview of the SM, starting with
192 the SM particle content, followed by a description of the electroweak interaction, the
193 Higgs boson and the associated production of Higgs boson and a single top quark
194 (tH). The description contained in this chapter is based on references [1–3].

195 2.2 Standard model of particle physics

196 Particle physics at the fundamental level is modeled in terms of a collection of in-
197 teracting particles and fields in a theory known as the “standard model of particle
198 physics (SM)”¹.

199 The full picture of the SM is composed of three fields², whose excitations are inter-
200 preted as particles called mediators or force-carriers; a set of fields, whose excitations
201 are interpreted as elementary particles, interacting through the exchange of those
202 mediators and a field that give the mass to elementary particles. Figure 2.1 shows an
203 scheme of the SM particles organization. In addition to the particles in the scheme,
204 their corresponding anti-particles, with opposite quantum numbers, are also part of
205 the picture; some particles are their own anti-particles, like photon or Higgs, or anti-
206 particle is already listed like in the W^+ and W^- case.

207

208 The mathematical formulation of the SM is based on group theory and the use of
209 Noether’s theorem [17] which states that for a physical system modeled by a La-
210 grangian that is invariant under a group of transformations a conservation law is
211 expected. For instance, a system described by a time-independent Lagrangian is
212 invariant (symmetric) under time changes (transformations) with the total energy
213 conservation law as the expected conservation law. In QED, the Q operator is the
214 generator of the $U(1)$ symmetry which according to the Noether’s theorem means
215 that there is a conserved charge; this conserved charge is the electric charge and thus
216 the law conservation of electric charge is established.

¹ The formal and complete treatment of the SM is out of the scope of this document, however a plenty of textbooks describing it at several levels are available in the literature. The treatment in “An Introduction To Quantum Field Theory (Frontiers in Physics)” by Michael E. Peskin and Dan V. Schroeder is quite comprehensive and detailed.

² Note that gravitational field is not included in the standard model formulation

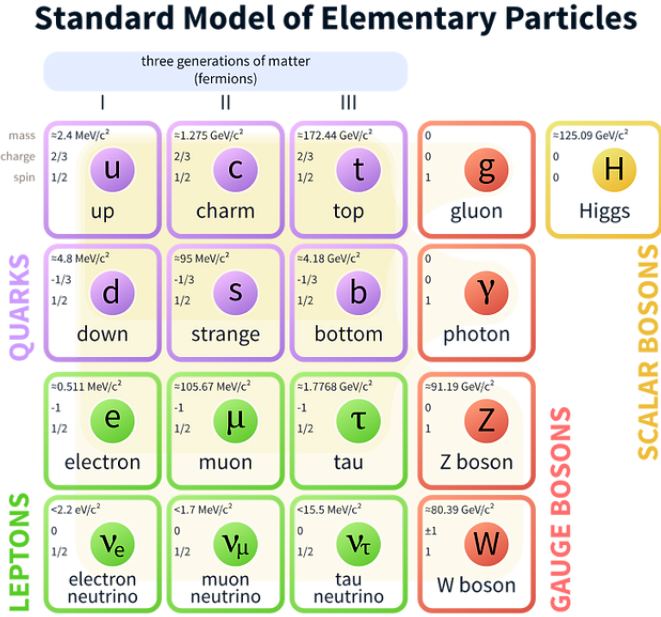


Figure 2.1: Schematic representation of the Standard model of particle physics. SM is a theoretical model intended to describe three of the four fundamental forces of the universe in terms of a set of particles and their interactions. [18].

217

- 218 In the SM, the symmetry group $SU(3)_C \otimes SU(2)_L \otimes U(1)_Y$ describes three of the
 219 four fundamental interactions in nature (see section 2.2.2): strong interaction (SI),
 220 weak interaction (WI) and electromagnetic interactions (EI) in terms of symmetries
 221 associated to physical quantities:
 222

 - Strong: $SU(3)_C$ associated to color charge
 - Weak: $SU(2)_L$ associated to weak isospin and chirality
 - Electromagnetic: $U(1)_Y$ associated to weak hypercharge and electric charge
 223
 224
 225 It will be shown that the electromagnetic and weak interactions are combined in
 226 the so-called electroweak interaction where chirality, hypercharge, weak isospin and
 227 electric charge are the central concepts.

228 2.2.1 Fermions

229 The basic constituents of the ordinary matter at the lowest level, which form the set
 230 of elementary particles in the SM formulation, are quarks and leptons. All of them
 231 have spin 1/2, therefore they are classified as fermions since they obey Fermi-Dirac
 232 statistics. In both cases, they come in six “flavors” and are organized in three gener-
 233 ations, or families, as shown in table 2.1.

234

235 There is a mass hierarchy between generations where the higher generation particles
 236 decays to the lower one which can explain why the ordinary matter is made of particles
 237 in the first generation. In the SM, neutrinos are modeled as massless particles so they
 238 are not subject to this mass hierarchy; however, today it is known that neutrinos are
 239 massive so the hierarchy could be restated. The reason behind this mass hierarchy is
 240 one of the most important open questions in particle physics, and it becomes more
 241 puzzling when noticing that the mass difference between first and second generation
 242 fermions is small compared to the mass difference with respect to the third generation.
 243 Usually, the second and third generation fermions are produced in high energy pro-
 244 cesses, like the ones recreated in the particle accelerators.

		Generation		
		1st	2nd	3rd
Leptons	Type	Electron (e)	Moun(μ)	Tau (τ)
	Charged Neutral	Electron neutrino (ν_e)	Muon neutrino (ν_μ)	Tau neutrino (ν_τ)
Quarks	Up-type Down-type	Up (u) Down (d)	Charm (c) Starnge (s)	Top (t) Bottom (b)

Table 2.1: Fermions of the SM. Quarks and leptons comes in six flavors each and are organized in three generations or families composed of two pairs of closely related particles. The close relationship is motivated by the fact that WI between leptons is limited to the members of the same generation. Generations differs by mass in a way that have been interpreted as a masss hierarchy.

245

246 **2.2.1.1 Leptons**

247 A lepton is an elementary particle that is not subject to the SI. As seen in table 2.1,
 248 there are two types of leptons, the charged ones (electron, muon and tau) and the
 249 neutral ones (the three neutrinos). The electric charge (Q) is the property that gives
 250 leptons the ability to participate in the EI. From the classical point of view, Q plays
 251 a central role determining, among others, the strength of the electric field through
 252 which the electromagnetic force is exerted. It is clear that neutrinos are not affected
 253 by EI because they don't carry electric charge.

254

255 Another feature of the leptons that is fundamental in the mathematical description
 256 of the SM is the chirality, which is closely related to spin and helicity. Helicity de-
 257 fine the handedness of a particle by relating its spin and momentum such that if
 258 they are parallel then the particle is right-handed; if spin and momentum are an-
 259 tiparallel the particle is said to be left-handed. The study of parity conservation
 260 (or violation) in β -decay have shown that only left-handed electrons/neutrinos or
 261 right-handed positrons/anti-neutrinos are created [19]; the inclusion of that feature
 262 in the theory was reached by using projection operators for helicity, however, helicity
 263 is frame dependent for massive particles which makes it not Lorentz invariant and
 264 then another related attribute has to be used: *chirality*.

265

266 Chirality is a purely quantum attribute which makes it not so easy to describe in
 267 graphical terms but it defines how the wave function of a particle transforms under
 268 certain rotations. As with helicity, there are two chiral states, left-handed chiral
 269 (L) and right-handed chiral (R). In the highly relativistic limit where $E \approx p \gg m$
 270 helicity and chirality converge, becoming exactly the same for massless particles. In

271 the following when referring to left-handed (right-handed) it means left-handed chiral
 272 (right-handed chiral). The fundamental fact about chirality is that while EI and SI
 273 are not sensitive to chirality, in WI left-handed and right-handed fermions are treated
 274 asymmetrically, such that only left handed fermions and right-handed anti-fermions
 275 are allowed to couple to WI mediators, which is a violation of parity. The way to
 276 translate this statement in a formal mathematical formulation is based on the isospin
 277 symmetry group $SU(2)_L$.

278 Each generation of leptons is seen as a weak isospin doublet.³ The left-handed charged
 279 lepton and its associated left-handed neutrino are arranged in doublets of weak isospin
 280 $T=1/2$ while their right-handed partners are singlets:

$$\begin{pmatrix} \nu_l \\ l \end{pmatrix}_L, l_R := \begin{pmatrix} \nu_e \\ e \end{pmatrix}_L, \begin{pmatrix} \nu_\mu \\ \mu \end{pmatrix}_L, \begin{pmatrix} \nu_\tau \\ \tau \end{pmatrix}_L, e_R, \mu_R, \tau_R, \nu_{eR}, \nu_{\mu R}, \nu_{\tau R} \quad (2.2)$$

281 The isospin third component refers to the eigenvalues of the weak isospin operator
 282 which for doublets is $T_3 = \pm 1/2$, while for singlets it is $T_3 = 0$. The physical meaning
 283 of this doublet-singlet arrangement falls in that the WI couples the two particles in
 284 the doublet by exchanging the interaction mediator while the singlet member is not
 285 involved in WI. The main properties of the leptons are summarized in table 2.2.

286

287 Altough all three flavor neutrinos have been observed, their masses remain unknown
 288 and only some estimations have been made [20]. The main reason is that the fla-
 289 vor eigenstates are not the same as the mass eigenstates which imply that when a
 290 neutrino is created its mass state is a linear combination of the three mass eigen-
 291 states and experiments can only probe the squared difference of the masses. The
 292 Pontecorvo-Maki-Nakagawa-Sakata (PMNS) mixing matrix encode the relationship

³ The weak isospin is an analogy of the isospin symmetry in strong interaction where neutron and proton are affected equally by strong force but differ in their charge.

293 between flavor and mass eigenstates.

Lepton	Q(e)	T_3	L_e	L_μ	L_τ	Mass (MeV/c ²)	Lifetime (s)
Electron (e)	-1	-1/2	1	0	0	0.5109989461(31)	Stable
Electron neutrino(ν_e)	0	1/2	1	0	0	Unknown	Unknown
Muon (μ)	-1	-1/2	0	1	0	105.6583745(24)	$2.1969811(22) \times 10^{-6}$
Muon neutrino (ν_μ)	0	1/2	0	1	0	Unknown	Unknown
Tau (τ)	-1	-1/2	0	0	1	1776.86(12)	$290.3(5) \times 10^{-15}$
Tau neutrino (τ_μ)	0	1/2	0	0	1	Unknown	Unknown

Table 2.2: Leptons properties [21]. Q: electric charge, T_3 : weak isospin. Only left-handed leptons and right-handed anti-leptons participate in the WI. Anti-particles with inverted T_3 , Q and lepton number complete the leptons set but are not listed. Right-handed leptons and left-handed anti-leptons, neither listed, form weak isospin singlets with $T_3 = 0$ and do not take part in the weak interaction.

294

295 2.2.1.2 Quarks

296 Quarks are the basic constituents of protons, neutrons and other non-elementary
 297 particles. The way quarks join to form bound states, called “hadrons”, is through the
 298 SI. Quarks are affected by all the fundamental interactions which means that they
 299 carry all the four types of charges: color, electric charge, weak isospin and mass.

Flavor	Q(e)	I_3	T_3	B	C	S	T	B'	Y	Color	Mass (MeV/c ²)
Up (u)	2/3	1/2	1/2	1/3	0	0	0	0	1/3	r,b,g	$2.2^{+0.6}_{-0.4}$
Charm (c)	2/3	0	1/2	1/3	1	0	0	0	4/3	r,b,g	$1.28 \pm 0.03 \times 10^3$
Top(t)	2/3	0	1/2	1/3	0	0	1	0	4/3	r,b,g	$173.1 \pm 0.6 \times 10^3$
Down(d)	-1/3	-1/2	-1/2	1/3	0	0	0	0	1/3	r,b,g	$4.7^{+0.5}_{-0.4}$
Strange(s)	-1/3	0	-1/2	1/3	0	-1	0	0	-2/3	r,b,g	96^{+8}_{-4}
Bottom(b)	-1/3	0	-1/2	1/3	0	0	0	-1	-2/3	r,b,g	$4.18^{+0.04}_{-0.03} \times 10^3$

Table 2.3: Quarks properties [21]. Q: electric charge, I_3 : isospin, T_3 : weak isospin, B: baryon number, C: charmness, S: strangeness, T: topness, B' : bottomness, Y: hypercharge. Anti-quarks posses the same mass and spin as quarks but all charges (color, flavor numbers) have opposite sign.

300

301 Table 2.3 summarizes the features of quarks, among which the most particular is
 302 their fractional electric charge. Note that fractional charge is not a problem, given
 303 that quarks are not found isolated, but serves to explain how composed particles are
 304 formed out of two or more valence quarks⁴.

305

306 Color charge is the responsible for the SI between quarks and is the symmetry
 307 ($SU(3)_C$) that defines the formalism to describe SI. There are three colors: red (r),
 308 blue(b) and green(g) and their corresponding three anti-colors; thus each quark carries
 309 one color unit while anti-quarks carries one anti-color unit. As said above, quarks are
 310 not allowed to be isolated due to the color confinement effect, therefore their features
 311 have been studied indirectly by observing their bound states created when:

312 • one quark with a color charge is attracted by an anti-quark with the correspond-
 313 ing anti-color charge forming a colorless particle called a “meson.”

314 • three quarks (anti-quarks) with different color (anti-color) charges are attracted
 315 among them forming a colorless particle called a “baryon(anti-baryon).”

316 In the first version of the quark model (1964), M. Gell-Mann [22] and G. Zweig [23,24]
 317 developed a consistent way to classify hadrons according to their properties. Only
 318 three quarks (u, d, s) were involved in a scheme in which all baryons have baryon
 319 number $B=1$ and therefore quarks have $B=1/3$; non-baryons have $B=0$. The scheme
 320 organize baryons in a two-dimensional space ($I_3 - Y$); Y (hypercharge) and I_3 (isospin)
 321 are quantum numbers related by the Gell-Mann-Nishijima formula [25, 26]:

$$Q = I_3 + \frac{Y}{2} \quad (2.3)$$

⁴ Hadrons can contain an indefinite number of virtual quarks and gluons, known as the quark and gluon sea, but only the valence quarks determine hadrons' quantum numbers.

322 where $Y = B + S + C + T + B'$ are the quantum numbers listed in table 2.3. Baryon
 323 number is conserved in SI and EI which means that single quarks cannot be created
 324 but in pairs $q - \bar{q}$.

325

326 Similar to leptons, there are six quark flavors organized in three generations (see table
 327 2.1) and follow a mass hierarchy which again implies that higher generations decay
 328 to first generation quarks.

	Quarks			T_3	Y_W	Leptons			T_3	Y_W
Doublets	$(\frac{u}{d'})_L$	$(\frac{c}{s'})_L$	$(\frac{t}{b'})_L$	$(\frac{1/2}{-1/2})$	1/3	$(\nu_e)_L$	$(\nu_\mu)_L$	$(\nu_\tau)_L$	$(\frac{1/2}{-1/2})$	-1
Singlets	u_R	c_R	t_R	0	4/3	ν_{eR}	$\nu_{\mu R}$	$\nu_{\tau R}$	0	-2

Table 2.4: Fermion weak isospin and weak hypercharge multiplets. Weak hypercharge is calculated through the Gell-Mann-Nishijima formula 2.3 but using the weak isospin and charge for quarks.

329

330 Isospin doublets of quarks are also defined (see table 2.4) and as for neutrinos, the
 331 mass eigenstates are not the same as the WI eigenstates which means that members of
 332 different quark generations are connected by the WI mediator; thus, up-type quarks
 333 are coupled not to down-type quarks directly but to a superposition of down-type
 334 quarks (q'_d) via WI according to:

$$q'_d = V_{CKM} q_d$$

335

$$\begin{pmatrix} d' \\ s' \\ b' \end{pmatrix} = \begin{pmatrix} V_{ud} & V_{us} & V_{ub} \\ V_{cd} & V_{cs} & V_{cb} \\ V_{td} & V_{ts} & V_{tb} \end{pmatrix} \begin{pmatrix} d \\ s \\ b \end{pmatrix} \quad (2.4)$$

336 where V_{CKM} is known as Cabibbo-Kobayashi-Maskawa (CKM) mixing matrix [27,28].

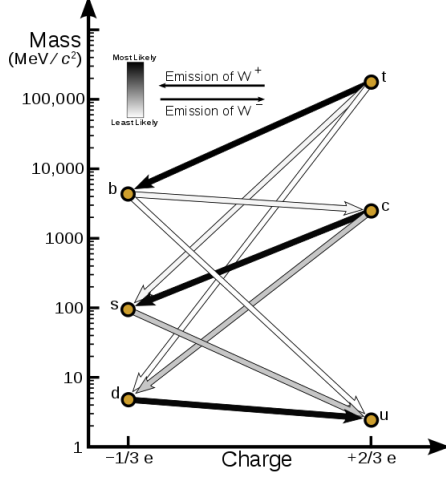


Figure 2.2: Transformations between quarks through WI. Higher generations quarks decay to first generation quarks by emitting a W boson. The arrow color indicates the likelihood of the transition according to the grey scale in the top left side which represent the CKM matrix parameters [29].

337 The weak decays of quarks are represented in the diagram of figure 2.2; again the
 338 CKM matrix plays a central role since it contains the probabilities for the different
 339 quark decay channels, in particular, note that quark decays are greatly favored be-
 340 tween generation members.

341

342 CKM matrix is a 3×3 unitary matrix parametrized by three mixing angles and the
 343 *CP-mixing phase*; the latter is the parameter responsible for the CP-violation in the
 344 SM. The fact that the b quark decays almost all the times to a top quark is exploited
 345 in this thesis when making the selection of the signal events by requiring the presence
 346 of a jet tagged as a jet coming from a b quark in the final state. The effect of the
 347 *CP-mixing phase* on the cross section of associated production of Higgs boson and a
 348 single top process is also explored in this thesis.

Fundamental interactions.

Illustration: Typoform

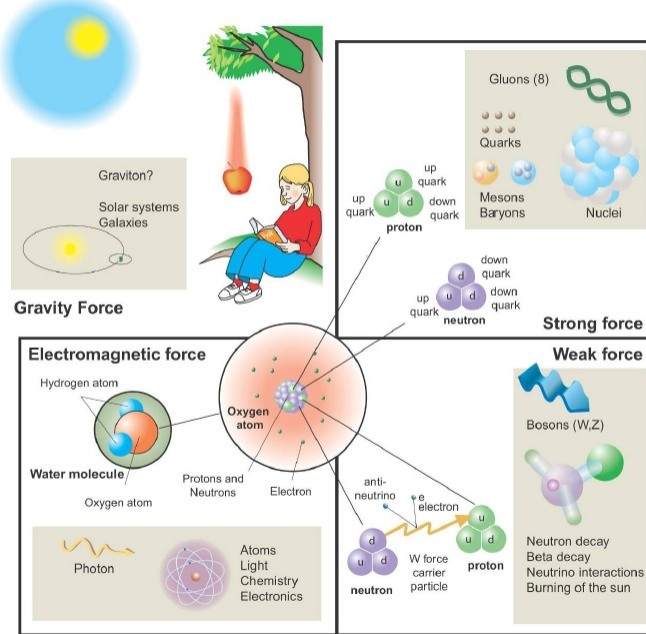


Figure 2.3: Fundamental interactions in nature. Despite the many manifestations of forces in nature, we can track all of them back to one of the fundamental interactions. The most common forces are gravity and electromagnetic given that all of us are subject and experience them in everyday life.

349 2.2.2 Fundamental interactions

350 Even though there are many manifestations of force in nature, like the ones represented in figure 2.3, we can classify all of them into one of four fundamental interactions:

- 353 • *Electromagnetic interaction (EI)* affect particles that are “electrically charged,”
 354 like electrons and protons. It is described by QED combining quantum mechanics,
 355 special relativity and electromagnetism in order to explain how particles
 356 with electric charge interact through the exchange of photons, therefore, one
 357 says that “Electromagnetic Force” is mediated by “photons”. Figure 2.4a) shows
 358 a graphical representation, known as “feynman diagram”, of electron-electron

359 scattering.

360 • *Strong interaction (SI)* described by Quantum Chromodynamics (QCD). Hadrons
 361 like proton and neutron have internal structure given that they are composed
 362 of two or more valence quarks⁵. Quarks have fractional electric charge which
 363 means that they are subject to electromagnetic interaction and in the case of the
 364 proton they should break apart due to electrostatic repulsion; however, quarks
 365 are held together inside the hadrons against their electrostatic repulsion by the
 366 “Strong Force” through the exchange of “gluons.” The analog to the electric
 367 charge is the “color charge”. Electrons and photons are elementary particles
 368 as quarks but they don’t carry color charge, therefore they are not subject to
 369 SI. The feynman diagram for gluon exchange between quarks is shown in figure
 370 2.4b).

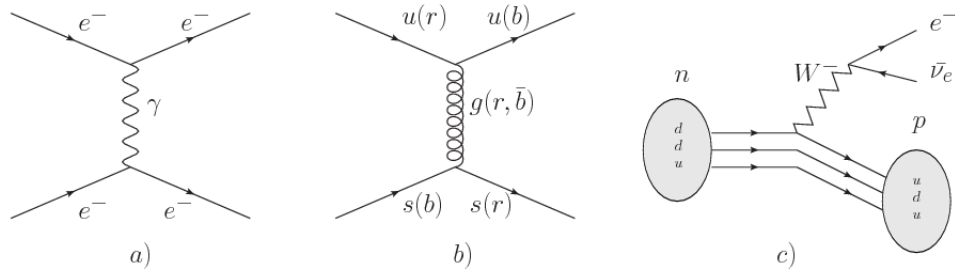


Figure 2.4: Feynman diagrams representing the interactions in SM; a) EI: e - e scattering; b) SI: gluon exchange between quarks ; c) WI: β -decay

371 • *Weak interaction (WI)* described by the Weak theory (WT), is responsible for
 372 instance for the radioactive decay in atoms and proton-proton (pp) fusion within
 373 the sun. Quarks and leptons are the particles affected by the weak interaction
 374 and posses a property called “flavor charge” which can be changed by emitting
 375 or absorbing one weak force mediator; they comes in six flavors each (see 2.2.1).
 376 There are three mediators of the “Weak force” known as “Z” boson in the case of

⁵ particles made of four and five quarks are exotic states not so common

377 electrically neutral changes and “ W^\pm ” bosons in the case of electrically charged
 378 changes. The “weak isospin” is the WI analog to electric charge in EI and color
 379 charge in SI and define how quarks and leptons are affected by the weak force.
 380 Figure 2.4c) shows the feynman diagram of β -decay where a newtron (n) is
 381 transformed in a proton (p) by emmiting a W^- particle. Since this thesis is in
 382 the frame of the electroweak interaction, a more detailed description of it will
 383 be given in section 2.3

384 • *Gravitational interaction (GI)* described by General Theory of Relativity (GR).
 385 It is responsible for the structure of galaxies and black holes as well as the
 386 expansion of the universe. As a classical theory, in the sense that it can be
 387 formulated without even appeal to the concept of quantization, it implies that
 388 the spacetime is a continuum and predictions can be made without limitation
 389 to the precision of the measurement tools which represent a direct contradiction
 390 of the quantum mechanics principles. Gravity is deterministic while quantum
 391 mechanics is probabilistic; despite that, efforts to develop a quantum theory of
 392 gravity have predicted the “graviton” as mediator of the Gravitational force⁶.

Interaction	Acts on	Relative strength	Range (m)	Mediators
Electromagnetic (QED)	Electrically charged particles	10^{-2}	Infinite	Photon
Strong (QCD)	Quarks and gluons	1	10^{-15}	Gluon
Weak (WI)	Leptons and quarks	10^{-6}	10^{-18}	W^\pm , Z
Gravitational (GI)	Massive particles	10^{-39}	Infinite	Graviton

Table 2.5: Fundamental interactions features [30].

393

394 Table 2.5 summarizes the main features of the fundamental interactions. The rela-
 395 tive strength of the fundamental forces reveals the meaning of strong and weak;

⁶ Actually a wide variety of theories have been developed in an attempt to describe gravity; some famous examples are string theory and supergravity.

396 a context where the relative strength of the SI is 1, the EI is about hundred times
 397 weaker and WI is about million times weaker than the SI. A good description on
 398 how the relative strength and range of the fundamental interactions are calculated
 399 can be found in references [30, 31]. In the everyday life, only EI and GI are explicitly
 400 experienced due to the range of these interactions; i.e., at the human scale distances
 401 only EI and GI have appreciable effects, in contrast to SI which at distances greater
 402 than 10^{-15} m become negligible.

403

404 QED was built successfully on the basis of the classical electrodynamics theory of
 405 Maxwell and Lorentz (CED), following theoretical and experimental requirements
 406 imposed by

- 407 • lorentz invariance: independence on the reference frame.
- 408 • locallity: interacting fields are evaluated at the same space-time point to avoid
 409 action at a distance.
- 410 • renormalizability: physical predictions are finite and well defined
- 411 • particle spectrum, symmetries and conservation laws already known must emerge
 412 from the theory.
- 413 • gauge invariance.

414 The gauge invariance requirement reflects the fact that the fundamental fields cannot
 415 be directly measured but associated fields which are the observables. Electric (“**E**”)
 416 and magnetic (“**B**”) fields in CED are associated with the electric scalar potential
 417 “**V**” and the vector potential “**A**”. In particular, **E** can be obtained by measuring
 418 the change in the space of the scalar potential (ΔV); however, two scalar potentials

419 differing by a constant “f” correspond to the same electric field. The same happens
 420 in the case of the vector potential “ \mathbf{A} ”; thus, different configurations of the associated
 421 fields result in the same set of values of the observables. The freedom in choosing
 422 one particular configuration is known as “gauge freedom”; the transformation law
 423 connecting two configurations is known as “gauge transformation” and the fact that
 424 the observables are not affected by a gauge transformation is called “gauge invariance”.
 425 When the gauge transformation:

$$\begin{aligned}\mathbf{A} &\rightarrow \mathbf{A} - \nabla f \\ V &\rightarrow V - \frac{\partial f}{\partial t}\end{aligned}\tag{2.5}$$

426 is applied to Maxwell equations, they are still satisfied and the fields remain invariant.
 427 Thus, the classical electrodynamics theory is invariant under gauge transformations
 428 and is called a “gauge theory”. The set of all gauge transformations form the “sym-
 429 metry group” of the theory, which according to the group theory, has a set of “group
 430 generators”. The number of group generators determine the number of “gauge fields”
 431 of the theory.

432

433 As mentioned in the first lines of section 2.2, QED has one symmetry group ($U(1)$)
 434 with one group generator (the Q operator) and one gauge field (the electromagnetic
 435 field A^μ). In CED there is not a clear definition, beyond the historical convention, of
 436 which fields are the fundamental and which are the associated, but in QED it is clear
 437 that the fundamental field is A^μ . When a gauge theory is quantized, the gauge field
 438 is quantized and its quanta is called “gauge boson”. The word boson characterize
 439 particles with integer spin which obey Bose-Einstein statistics.

440

441 As will be detailed in section 2.3, interactions between particles in a system can be
 442 obtained by considering first the Lagrangian density of free particles in the system,
 443 which of course is incomplete because the interaction terms have been left out, and
 444 demanding global phase transformation invariance. Global phase transformation in-
 445 variance means that a gauge transformation is performed identically to every point
 446 in the space⁷ and the Lagrangian remains invariant. Then, the global transformation
 447 is promoted to a local phase transformation (this time the gauge transformation de-
 448 pends on the position in space) and again invariance is required.

449

450 Due to the space dependence of the local transformation, the Lagrangian density is
 451 not invariant anymore. In order to restate the gauge invariance, the gauge covariant
 452 derivative is introduced in the Lagrangian and with it the gauge field responsible for
 453 the interaction between particles in the system. The new Lagrangian density is gauge
 454 invariant, includes the interaction terms needed to account for the interactions and
 455 provide a way to explain the interaction between particles through the exchange of
 456 the gauge boson.

457 This recipe was used to build QED and the theories that aim to explain the funda-
 458 mental interactions.

459 **2.2.3 Gauge Bosons**

460 The importance of the gauge bosons comes from the fact that they are the force
 461 mediators or force carriers. The features of the gauge bosons reflect the features of
 462 the fields they represent; these features are extracted from the Lagrangian density used
 463 to describe the interactions. In section 2.3, it will be shown how the gauge bosons

⁷ Here space corresponds to the 4-dimensional space i.e. space-time.

464 of the EI and WI emerge from the electroweak Lagrangian. The SI gauge bosons
 465 features are also extracted from the SI Lagrangian but it is not detailed in this
 466 document. Here, the main features of the SM gauge bosons will be briefly presented
 467 and summarized in table 2.6.

468 • **Photon.** EI occurs when the photon couples to (is exchanged between) particles
 469 carrying electric charge; however, the photon itself does not carry electric charge,
 470 therefore, there is no coupling between photons. Given that the photon is
 471 massless the EI is of infinite range i.e. electrically charged particles interact
 472 even if they are located far away one from each other; that also means that
 473 photons always move with the speed of light.

474 • **Gluon.** SI is mediated by gluons, which same as photons are massless. They
 475 carry one unit of color charge and one unit of anticolor charge which means that
 476 gluons couples to other gluons. As a result, the range of the SI is not infinite
 477 but very short due to the attraction between gluons, giving rise to the “color
 478 confinement” which explains why color charged particles cannot be isolated but
 479 live within composited particles, like quarks inside protons.

480 • **W, Z.** The EWI mediators, W^\pm and Z, are massive which explain its short-
 481 range. Given that the WI is the only interaction that can change the flavor
 482 of the interacting particles, the W boson is the responsible for the nuclear
 483 transmutation where a neutron is converted in a proton or vice versa with the
 484 involvement of an electron and a neutrino. The Z boson is the responsible of the
 485 neutral weak processes like neutrino elastic scattering where no electric charge
 486 but momentum transference is involved. WI gauge bosons carry isospin charge
 487 which makes possible the interaction between them.

Interaction	Mediator	Electric charge (e)	Color charge	Weak Isospin	mass (GeV/c ²)
Electromagnetic	Photon (γ)	0	No	0	0
Strong	Gluon (g)	0	Yes -octet	No	0
Weak	W^\pm Z	± 1 0	No No	± 1 0	80.385 ± 0.015 91.188 ± 0.002

Table 2.6: SM gauge bosons main features [21].

488

489 **2.3 Electroweak unification and the Higgs**

490 **mechanism**

491 Physicist dreams of building a theory that contains all the interactions in one single
 492 interaction, i.e. showing that at some scale in energy all the four fundamental in-
 493 teractions are unified and only one interaction emerges in a “Theory of everything”.
 494 The first sign of the feasibility of such unification comes from success in the con-
 495 struction of the CED. Einstein spent years trying to reach that dream, which by
 496 1920 only involved electromagnetism and gravity, with no success; however, a new
 497 partial unification was achieved in the 1960’s, when S.Glashow [14], A.Salam [15] and
 498 S.Weinberg [16] independently proposed that electromagnetic and weak interactions
 499 are two manifestations of a more general interaction called “electroweak interaction.”
 500 QCD and EWT were developed in parallel and following the useful prescription pro-
 501 vided by QED and the gauge invariance principles.

502

503 The theory of weak interactions was capable of explaining the β -decay and in general
 504 the processes mediated by W^\pm bosons. However, there were some processes like the
 505 “ $\nu_\mu - e$ scattering” which would require the exchange of two W bosons (see figure 2.5
 506 top diagrams) giving rise to divergent loop integrals and then non finite predictions.

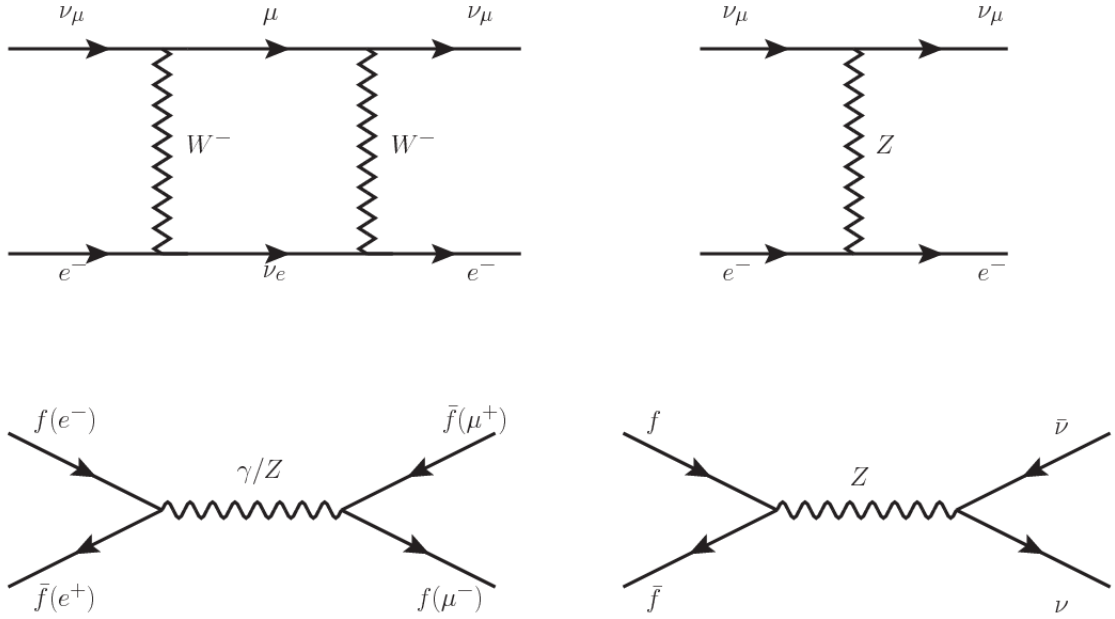


Figure 2.5: Top: $\nu_\mu - e^-$ scattering going through charged currents (left) and neutral currents (right). Bottom: neutral current processes for charged fermions (left) and involving neutrinos (right). While neutral current processes involving only charged fermions can proceed through EI or WI, those involving neutrinos can only proceed via WI.

507 By including neutral currents involving fermions via the exchange of neutral bosons
 508 Z , those divergences are compensated and the predictions become realistic.
 509 Neutral weak interaction vertices conserve flavor in the same way as the electromag-
 510 netic vertices do, but additionally, the Z boson can couple to neutrinos which implies
 511 that processes involving charged fermions can proceed through EI or WI but processes
 512 involving neutrinos can proceed only through WI.

513

514 The prescription to build a gauge theory of the WI consist of proposing a free field La-
 515 grangian density that includes the particles involved; next, by requesting invariance
 516 under global phase transformations first and generalizing to local phase transfor-
 517 mations invariance later, the conserved currents are identified and interactions are
 518 generated by introducing gauge fields. Given that the goal is to include the EI and

519 WI in a single theory, the group symmetry considered should be a combination of
 520 $SU(2)_L$ and $U(1)_{em}$, however the latter cannot be used directly because the EI treat
 521 left and right-handed particles indistinctly in contrast to the former. Fortunately, the
 522 weak hypercharge, which is a combination of the weak isospin and the electric charge
 523 (eqn 2.3) is suitable to be used since it is conserved by the EI and WI. Thus, the
 524 symmetry group to be considered is

$$G \equiv SU(2)_L \otimes U(1)_Y \quad (2.6)$$

525 The following treatment applies to any of the fermion generations but for simplicity
 526 the first generation of leptons will be considered [2, 3, 32, 33]. Also, the unified weak
 527 and electromagnetic interaction will be referred as “Electroweak Interaction (EWI).”
 528 Given the first generation of leptons

$$\psi_1 = \begin{pmatrix} \nu_e \\ e^- \end{pmatrix}_L, \quad \psi_2 = \nu_{eR}, \quad \psi_3 = e_R^- \quad (2.7)$$

529 the charged fermionic currents are given by

$$J_\mu \equiv J_\mu^+ = \bar{\nu}_{eL} \gamma_\mu e_L, \quad J_\mu^\dagger \equiv J_\mu^- = \bar{e}_L \gamma_\mu \nu_{eL} \quad (2.8)$$

530 and the free Lagrangian is given by

$$\mathcal{L}_0 = \sum_{j=1}^3 i\bar{\psi}_j(x) \gamma^\mu \partial_\mu \psi_j(x). \quad (2.9)$$

531 Mass terms are included directly in the QED and QCD free Lagrangians since they
 532 preserve the invariance under the symmetry transformations involved which treat
 533 left-handed and right-handed similarly, however mass terms of the form

$$m_W^2 W_\mu^\dagger(x) W^\mu(x) + \frac{1}{2} m_Z^2 Z_\mu(x) Z^\mu(x) - m_e \bar{\psi}_e(x) \psi_e(x) \quad (2.10)$$

534 which represent the mass of W^\pm , Z and electrons, are not invariant under G trans-
 535 formations, therefore the gauge fields described by the EWI are in principle massless.

536

537 Experiments have shown that the gauge fields are not massless; however, they have
 538 to acquire mass through a mechanism compatible with the gauge invariance; that
 539 mechanism is known as the “Higgs mechanism” and will be considered later in this
 540 section. The global transformations in the combined symmetry group G can be
 541 written as

$$\begin{aligned} \psi_1(x) &\xrightarrow{G} \psi'_1(x) \equiv U_Y U_L \psi_1(x), \\ \psi_2(x) &\xrightarrow{G} \psi'_2(x) \equiv U_Y \psi_2(x), \\ \psi_3(x) &\xrightarrow{G} \psi'_3(x) \equiv U_Y \psi_3(x) \end{aligned} \quad (2.11)$$

542 where U_L represent the $SU(2)_L$ transformation acting on the weak isospin doublet
 543 only and U_Y represent the $U(1)_Y$ transformation acting on all the weak isospin mul-
 544 tiplets. Explicitly

$$U_L \equiv \exp\left(i \frac{\sigma_i}{2} \alpha^i\right), \quad U_Y \equiv \exp(i y_i \beta) \quad (i = 1, 2, 3) \quad (2.12)$$

545 with σ_i the Pauli matrices and y_i the weak hypercharges. In order to promote the
 546 transformations from global to local while keeping the invariance, it is required that
 547 $\alpha^i = \alpha^i(x)$, $\beta = \beta(x)$ and the replacement of the ordinary derivatives by the covariant
 548 derivatives

$$\begin{aligned}
D_\mu \psi_1(x) &\equiv \left[\partial_\mu + ig\sigma_i W_\mu^i(x)/2 + ig'y_1 B_\mu(x) \right] \psi_1(x) \\
D_\mu \psi_2(x) &\equiv \left[\partial_\mu + ig'y_2 B_\mu(x) \right] \psi_2(x) \\
D_\mu \psi_3(x) &\equiv \left[\partial_\mu + ig'y_3 B_\mu(x) \right] \psi_3(x)
\end{aligned} \tag{2.13}$$

549 introducing in this way four gauge fields, $W_\mu^i(x)$ and $B_\mu(x)$, in the process. The
550 covariant derivatives (eqn 2.13) are required to transform in the same way as fermion
551 fields $\psi_i(x)$ themselves, therefore, the gauge fields transform as:

$$\begin{aligned}
B_\mu(x) &\xrightarrow{G} B'_\mu(x) \equiv B_\mu(x) - \frac{1}{g'} \partial_\mu \beta(x) \\
W_\mu^i(x) &\xrightarrow{G} W_\mu^{i\prime}(x) \equiv W_\mu^i(x) - \frac{i}{g} \partial_\mu \alpha_i(x) - \varepsilon_{ijk} \alpha_i(x) W_\mu^j(x).
\end{aligned} \tag{2.14}$$

552 The G invariant version of the Lagrangian density 2.9 can be written as

$$\mathcal{L}_0 = \sum_{j=1}^3 i\bar{\psi}_j(x) \gamma^\mu D_\mu \psi_j(x) \tag{2.15}$$

553 where free massless fermion and gauge fields and fermion-gauge boson interactions
554 are included. The EWI Lagrangian density must additionally include kinetic terms
555 for the gauge fields (\mathcal{L}_G) which are built from the field strengths, according to

$$B_{\mu\nu}(x) \equiv \partial_\mu B_\nu - \partial_\nu B_\mu \tag{2.16}$$

$$W_{\mu\nu}^i(x) \equiv \partial_\mu W_\nu^i(x) - \partial_\nu W_\mu^i(x) - g\varepsilon^{ijk} W_\mu^j W_\nu^k \tag{2.17}$$

556 the last term in eqn. 2.17 is added in order to hold the gauge invariance; therefore,

$$\mathcal{L}_G = -\frac{1}{4}B_{\mu\nu}(x)B^{\mu\nu}(x) - \frac{1}{4}W_{\mu\nu}^i(x)W_i^{\mu\nu}(x) \quad (2.18)$$

557 which contains not only the free gauge fields contributions but also the gauge fields
 558 self-interactions and interactions among them.

559 The three weak isospin conserved currents resulting from the $SU(2)_L$ symmetry are
 560 given by

$$J_\mu^i(x) = \frac{1}{2}\bar{\psi}_1(x)\gamma_\mu\sigma^i\psi_1(x) \quad (2.19)$$

561 while the weak hypercharge conserved current resulting from the $U(1)_Y$ symmetry is
 562 given by

$$J_\mu^Y = \sum_{j=1}^3 \bar{\psi}_j(x)\gamma_\mu y_j\psi_j(x) \quad (2.20)$$

563 In order to evaluate the electroweak interactions modeled by an isotriplet fields W_μ^i
 564 which couples to isospin currents J_μ^i with strength g and additionally the singlet
 565 field B_μ which couples to the weak hypercharge current J_μ^Y with strength $g'/2$, the
 566 interaction Lagrangian density to be considered is

$$\mathcal{L}_I = -g J^{i\mu}(x) W_\mu^i(x) - \frac{g'}{2} J^Y{}^\mu(x) B_\mu(x) \quad (2.21)$$

567 Note that the weak isospin currents are not the same as the charged fermionic currents
 568 that were used to describe the WI (eqn 2.8), since the weak isospin eigenstates are
 569 not the same as the mass eigenstates, but they are closely related

$$J_\mu = \frac{1}{2}(J_\mu^1 + iJ_\mu^2), \quad J_\mu^\dagger = \frac{1}{2}(J_\mu^1 - iJ_\mu^2). \quad (2.22)$$

570 The same happen with the gauge fields W_μ^i which are related to the mass eigenstates
 571 W^\pm by

$$W_\mu^+ = \frac{1}{\sqrt{2}}(W_\mu^1 - iW_\mu^2), \quad W_\mu^- = \frac{1}{\sqrt{2}}(W_\mu^1 + iW_\mu^2). \quad (2.23)$$

572 The fact that there are three weak isospin conserved currents is an indication that in
 573 addition to the charged fermionic currents which couple charged to neutral leptons
 574 there should be a neutral fermionic current that couples neutral fermions or electri-
 575 cally charged fermions that has the same electric charge and thus does not imply
 576 electric charge change. The third weak isospin current contains a term that is simi-
 577 lar to the electromagnetic current (j_μ^{em}), indicating that there is a relation between
 578 them and resembling the Gell-Mann-Nishijima formula 2.3 adapted to electroweak
 579 interactions

$$Q = T_3 + \frac{Y_W}{2}. \quad (2.24)$$

580 Just as Q generates the $U(1)_{em}$ symmetry, the weak hypercharge generates the $U(1)_Y$
 581 symmetry as said before. It is possible to write the relationship in terms of the currents
 582 as

$$j_\mu^{em} = J_\mu^3 + \frac{1}{2}J_\mu^Y. \quad (2.25)$$

583 The neutral gauge fields W_μ^3 and B_μ cannot be directly identified with the Z and the
 584 photon fields since the photon interacts similarly with left and right-handed fermions;
 585 however, they are related through a linear combination given by

$$A_\mu = B_\mu \cos \theta_W + W_\mu^3 \sin \theta_W \quad (2.26)$$

$$Z_\mu = -B_\mu \sin \theta_W + W_\mu^3 \cos \theta_W$$

586 where θ_W is known as the “Weinberg angle.” The interaction Lagrangian is now given

587 by

$$\mathcal{L}_I = -\frac{g}{\sqrt{2}}(J^\mu W_\mu^+ + J^{\mu\dagger} W_\mu^-) - \left(g \sin \theta_W J_\mu^3 + g' \cos \theta_W \frac{J_\mu^Y}{2}\right) A^\mu - \left(g \cos \theta_W J_\mu^3 - g' \sin \theta_W \frac{J_\mu^Y}{2}\right) Z^\mu \quad (2.27)$$

588 the first term is the weak charged current interaction, while the second term is the

589 electromagnetic interaction under the condition

$$g \sin \theta_W = g' \cos \theta_W = e, \quad \frac{g'}{g} = \tan \theta_W \quad (2.28)$$

590 contained in the eqn.2.25; the third term is the neutral weak current.

591 Note that the neutral fields transformation given by the eqn. 2.26 can be written in

592 terms of the coupling constants g and g' as:

$$A_\mu = \frac{g' W_\mu^3 + g B_\mu}{\sqrt{g^2 + g'^2}}, \quad Z_\mu = \frac{g W_\mu^3 - g' B_\mu}{\sqrt{g^2 + g'^2}} \quad (2.29)$$

593 So far, the Lagrangian density describing the non-massive EWI is:

$$\mathcal{L}_{nmEWI} = \mathcal{L}_0 + \mathcal{L}_G \quad (2.30)$$

594 where fermion and gauge fields have been considered massless because their regular

595 mass terms are manifestly non invariant under G transformations; therefore, masses

596 have to be generated in a gauge invariant way. The mechanism by which this goal is

597 achieved is known as the “Higgs mechanism” and is closely connected to the concept
 598 of “spontaneous symmetry breaking.”

599 2.3.1 Spontaneous symmetry breaking

600 Figure 2.6 left shows a steel nail (top) which is subject to an external force; the form
 of the potential energy is also shown (bottom).

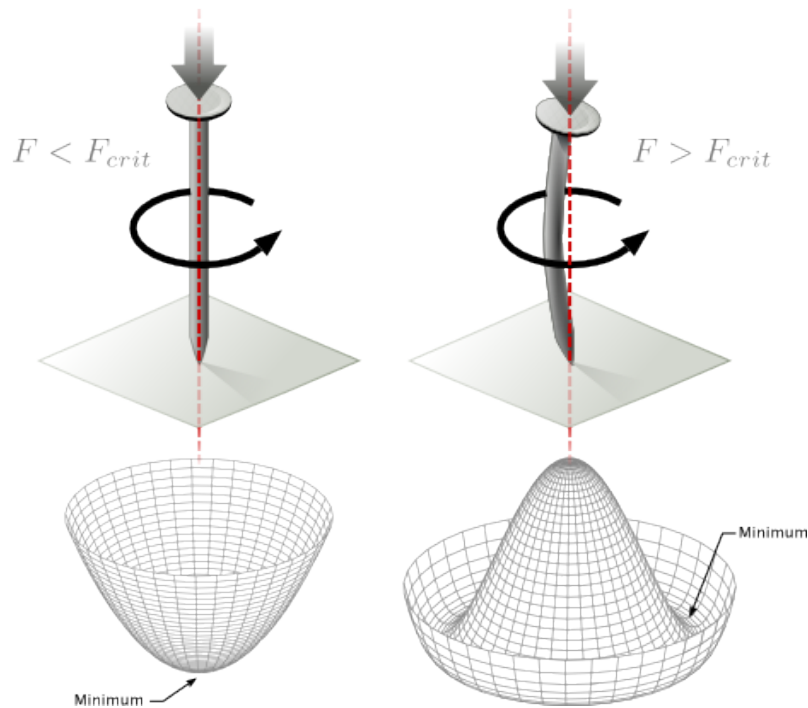


Figure 2.6: Spontaneous symmetry breaking mechanism. The steel nail, subject to an external force (top left), has rotational symmetry with respect to its axis. When the external force overcomes a critical value the nail buckles (top right) choosing a minimal energy state (ground state) and thus “*breaking spontaneously the rotational symmetry*”. The potential energy (bottom) changes but holds the rotational symmetry; however, an infinite number of asymmetric ground states are generated and circularly distributed in the bottom of the potential [34].

601
 602 Before reaching the critical force value, the system has rotational symmetry with re-
 603 spect to the nail axis; however, after the critical force value is reached the nail buckles
 604 (top right). The form of the potential energy (bottom right) changes, preserving its

605 rotational symmetry although its minima do not exhibit that rotational symmetry
 606 any longer. Right before the nail buckles there is no indication of the direction the
 607 nail will bend because any of the directions are equivalent, but once the nail bent,
 608 choosing a direction, an arbitrary minimal energy state (ground state) is selected and
 609 it does not share the system rotational symmetry. This mechanism for reaching an
 610 asymmetric ground state is known as “*spontaneous symmetry breaking (SSB)*”.
 611 The lesson from this analysis is that the way to introduce the SSB mechanism into a
 612 system is by adding the appropriate potential to it.

613

614 Figure 2.7 shows a plot of the potential $V(\phi)$ in the case of a scalar field ϕ

$$V(\phi) = \mu^2 \phi^\dagger \phi + \lambda (\phi^\dagger \phi)^2 \quad (2.31)$$

615 If $\mu^2 > 0$ the potential has only one minimum at $\phi = 0$ and describe a scalar field
 616 with mass μ . If $\mu^2 < 0$ the potential has a local maximum at $\phi = 0$ and two minima
 617 at $\phi = \pm\sqrt{-\mu^2/\lambda}$ which enables the SSB mechanism to work.

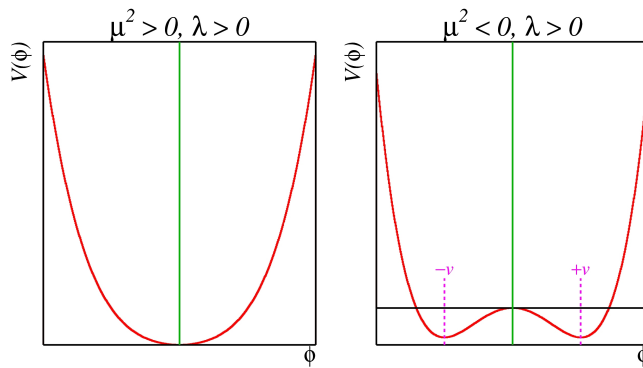


Figure 2.7: Shape of the potential $V(\phi)$ for $\lambda > 0$ and: $\mu^2 > 0$ (left) and $\mu^2 < 0$ (right). The case $\mu^2 < 0$ corresponds to the potential suitable for introducing the SSB mechanism by choosing one of the two ground states which are connected via reflection symmetry. [34].

618 In the case of a complex scalar field $\phi(x)$

$$\phi(x) = \frac{1}{\sqrt{2}}(\phi_1 + i\phi_2) \quad (2.32)$$

the Lagrangian (invariant under global $U(1)$ transformations) is given by

$$\mathcal{L} = (\partial_\mu \phi)^\dagger (\partial^\mu \phi) - V(\phi), \quad V(\phi) = \mu^2 \phi^\dagger \phi + \lambda (\phi^\dagger \phi)^2 \quad (2.33)$$

where an appropriate potential has been added in order to introduce the SSB.

As seen in figure 2.8, the potential has now an infinite number of minima circularly distributed along the ξ -direction which makes possible the occurrence of the SSB by choosing an arbitrary ground state; for instance, $\xi = 0$, i.e. $\phi_1 = v, \phi_2 = 0$

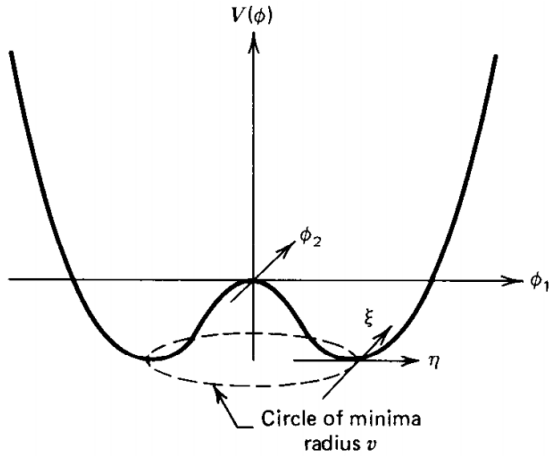


Figure 2.8: Potential for complex scalar field. There is a circle of minima of radius v along the ξ -direction [3].

$$\phi_0 = \frac{v}{\sqrt{2}} \exp(i\xi) \xrightarrow{\text{SSB}} \phi_0 = \frac{v}{\sqrt{2}} \quad (2.34)$$

As usual, excitations over the ground state are studied by making an expansion about it; thus, the excitation can be parametrized as:

$$\phi(x) = \frac{1}{\sqrt{2}}(v + \eta(x) + i\xi(x)) \quad (2.35)$$

626 which when substituted into eqn. 2.33 produces a Lagrangian in terms of the new
 627 fields η and ξ

$$\mathcal{L}' = \frac{1}{2}(\partial_\mu \xi)^2 + \frac{1}{2}(\partial_\mu \eta)^2 + \mu^2 \eta^2 - V(\phi_0) - \lambda v \eta (\eta^2 + \xi^2) - \frac{\lambda}{4}(\eta^2 + \xi^2)^2 \quad (2.36)$$

628 where the last two terms represent the interactions and self-interaction between the
 629 two fields η and ξ . The particular feature of the SSB mechanism is revealed when
 630 looking to the first three terms of \mathcal{L}' . Before the SSB, only the massless ϕ field is
 631 present in the system; after the SSB there are two fields of which the η -field has
 632 acquired mass $m_\eta = \sqrt{-2\mu^2}$ while the ξ -field is still massless (see figure 2.9).

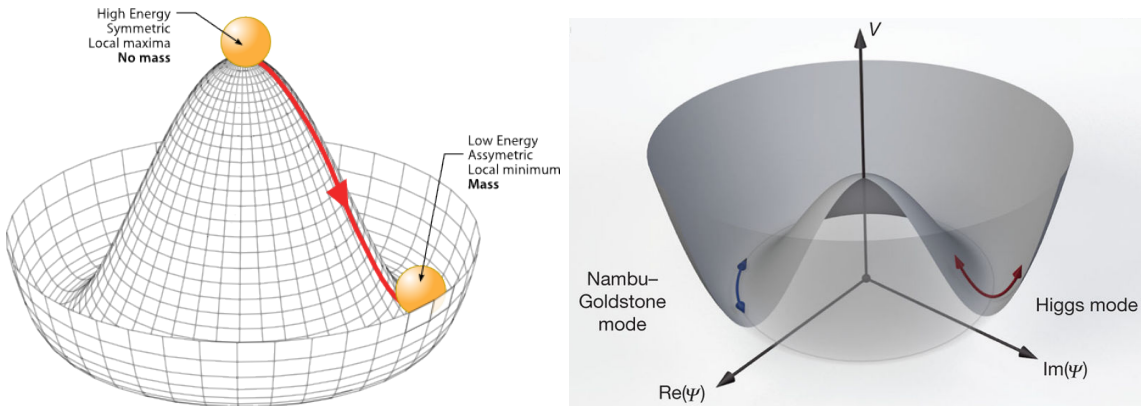


Figure 2.9: SSB mechanism for a complex scalar field [34, 35].

633 Thus, the SSB mechanism serves as a method to generate mass but as a side effect a
 634 massless field is introduced in the system. This fact is known as the Goldstone theorem
 635 and states that a massless scalar field appears in the system for each continuous
 636 symmetry spontaneously broken. Another version of the Goldstone theorem states
 637 that “if a Lagrangian is invariant under a continuous symmetry group G , but the
 638 vacuum is only invariant under a subgroup $H \subset G$, then there must exist as many
 639 massless spin-0 particles (Nambu-Goldstone bosons) as broken generators.” [33] The

640 Nambu-Goldstone boson can be understood considering that the potential in the ξ -
 641 direction is flat so excitations in that direction are not energy consuming and thus
 642 represent a massless state.

643 2.3.2 Higgs mechanism

644 When the SSB mechanism is introduced in the formulation of the EWI in an attempt
 645 to generate the mass of the so far massless gauge bosons and fermions, an interesting
 646 effect is revealed. In order to keep the G symmetry group invariance and generate
 647 the mass of the EW gauge bosons a G invariant Lagrangian density (\mathcal{L}_S) has to be
 648 added to the non massive EWI Lagrangian (eqn. 2.30)

$$\mathcal{L}_S = (D_\mu \phi)^\dagger (D^\mu \phi) - \mu^2 \phi^\dagger \phi - \lambda (\phi^\dagger \phi)^2, \quad \lambda > 0, \mu^2 < 0 \quad (2.37)$$

$$D_\mu \phi = \left(i\partial_\mu - g \frac{\sigma_i}{2} W_\mu^i - g' \frac{Y}{2} B_\mu \right) \phi \quad (2.38)$$

649 ϕ has to be an isospin doublet of complex scalar fields so it preserves the G invariance;
 650 thus ϕ can be defined as:

$$\phi = \begin{pmatrix} \phi^+ \\ \phi^0 \end{pmatrix} \equiv \frac{1}{\sqrt{2}} \begin{pmatrix} \phi_1 + i\phi_2 \\ \phi_3 + i\phi_4 \end{pmatrix}. \quad (2.39)$$

651 The minima of the potential are defined by

$$\phi^\dagger \phi = \frac{1}{2} (\phi_1^2 + \phi_2^2 + \phi_3^2 + \phi_4^2) = -\frac{\mu^2}{2\lambda}. \quad (2.40)$$

652 The choice of the ground state is critical. By choosing a ground state, invariant under
 653 $U(1)_{em}$ gauge symmetry, the photon will remain massless and the W^\pm and Z bosons
 654 masses will be generated which is exactly what is needed. In that sense, the best

655 choice corresponds to a weak isospin doublet with $T_3 = -1/2$, $Y_W = 1$ and $Q = 0$
 656 which defines a ground state with $\phi_1 = \phi_2 = \phi_4$ and $\phi_3 = v$:

$$\phi_0 \equiv \frac{1}{\sqrt{2}} \begin{pmatrix} 0 \\ v \end{pmatrix}, \quad v^2 \equiv -\frac{\mu^2}{\lambda}. \quad (2.41)$$

657 where the vacuum expectation value v is fixed by the Fermi coupling G_F according
 658 to $v = (\sqrt{2}G_F)^{1/2} \approx 246$ GeV.

659 The G symmetry has been broken and three Nambu-Goldstone bosons will appear.
 660 The next step is to expand ϕ about the chosen ground state as:

$$\phi(x) = \frac{1}{\sqrt{2}} \exp\left(\frac{i}{v} \sigma_i \theta^i(x)\right) \begin{pmatrix} 0 \\ v + H(x) \end{pmatrix} \approx \frac{1}{\sqrt{2}} \begin{pmatrix} \theta_1(x) + i\theta_2(x) \\ v + H(x) - i\theta_3(x) \end{pmatrix} \quad (2.42)$$

661 to describe fluctuations from the ground state ϕ_0 . The fields $\theta_i(x)$ represent the
 662 Nambu-Goldstone bosons while $H(x)$ is known as “higgs field.” The fundamental
 663 feature of the parametrization used is that the dependence on the $\theta_i(x)$ fields is
 664 factored out in a global phase that can be eliminated by taking the physical “unitary
 665 gauge” $\theta_i(x) = 0$. Therefore the expansion about the ground state is given by:

$$\phi(x) \frac{1}{\sqrt{2}} \begin{pmatrix} 0 \\ v + H(x) \end{pmatrix} \quad (2.43)$$

666 which when substituted into \mathcal{L}_S (eqn. 2.37) results in a Lagrangian containing the now
 667 massive three gauge bosons W^\pm, Z , one massless gauge boson (photon) and the new
 668 Higgs field (H). The three degrees of freedom corresponding to the Nambu-Goldstone
 669 bosons are now integrated into the massive gauge bosons as their longitudinal polar-
 670 izations which were not available when they were massless particles. The effect by
 671 which vector boson fields acquire mass after an spontaneous symmetry breaking but
 672 without an explicit gauge invariance breaking is known as the “*Higgs mechanism*.”

673 The mechanism was proposed by three independent groups: F.Englert and R.Brout
 674 in August 1964 [36], P.Higgs in October 1964 [37] and G.Guralnik, C.Hagen and
 675 T.Kibble in November 1964 [38]; however, its importance was not realized until
 676 S.Glashow [14], A.Salam [15] and S.Weinberg [16] independently proposed that elec-
 677 tromagnetic and weak interactions are two manifestations of a more general interac-
 678 tion called “electroweak interaction” in 1967.

679 2.3.3 Masses of the gauge bosons

680 The mass of the gauge bosons is extracted by evaluating the kinetic part of Lagrangian
 681 \mathcal{L}_S in the ground state (known also as the vacuum expectation value) i.e.

$$\left| \left(\partial_\mu - ig \frac{\sigma_i}{2} W_\mu^i - i \frac{g'}{2} B_\mu \right) \phi_0 \right|^2 = \left(\frac{1}{2} v g \right)^2 W_\mu^+ W^{-\mu} + \frac{1}{8} v^2 (W_\mu^3, B_\mu) \begin{pmatrix} g^2 & -gg' \\ -gg' & g'^2 \end{pmatrix} \begin{pmatrix} W^{3\mu} \\ B^\mu \end{pmatrix} \quad (2.44)$$

682 comparing with the typical mass term for a charged boson $M_W^2 W^+ W^-$

$$M_W = \frac{1}{2} v g. \quad (2.45)$$

The second term in the right side of the eqn.2.44 comprises the masses of the neutral
 bosons, but it needs to be written in terms of the gauge fields Z_μ and A_μ in order to
 be compared to the typical mass terms for neutral bosons, therefore using eqn. 2.29

$$\begin{aligned} \frac{1}{8} v^2 [g^2 (W_\mu^3)^2 - 2gg' W_\mu^3 B^\mu + g'^2 B_\mu^2] &= \frac{1}{8} v^2 [g W_\mu^3 - g' B_\mu]^2 + 0[g' W_\mu^3 + g B_\mu]^2 \quad (2.46) \\ &= \frac{1}{8} v^2 [\sqrt{g^2 + g'^2} Z_\mu]^2 + 0[\sqrt{g^2 + g'^2} A_\mu]^2 \end{aligned}$$

683 and then

$$M_Z = \frac{1}{2}v\sqrt{g^2 + g'^2}, \quad M_A = 0 \quad (2.47)$$

684 2.3.4 Masses of the fermions

685 The lepton mass terms can be generated by introducing a gauge invariant Lagrangian
 686 term describing the Yukawa coupling between the lepton field and the Higgs field:

$$\mathcal{L}_{Yl} = -G_l \left[(\bar{\nu}_l, \bar{l})_L \begin{pmatrix} \phi^+ \\ \phi^0 \end{pmatrix} l_R + \bar{l}_R (\phi^-, \bar{\phi}^0) \begin{pmatrix} \nu_l \\ l \end{pmatrix} \right], \quad l = e, \mu, \tau. \quad (2.48)$$

687 After the SSB and replacing the usual field expansion about the ground state (eqn.2.41)
 688 into \mathcal{L}_{Yl} , the mass term arises

$$\mathcal{L}_{Yl} = -m_l(\bar{l}_L l_R + \bar{l}_R l_L) - \frac{m_l}{v}(\bar{l}_L l_R + \bar{l}_R l_L)H = -m_l \bar{l}l \left(1 + \frac{H}{v}\right) \quad (2.49)$$

689

$$m_l = \frac{G_l}{\sqrt{2}}v \quad (2.50)$$

690 where the additional term represents the lepton-Higgs interaction. The quark masses
 691 are generated in a similar way as lepton masses but for the upper member of the
 692 quark doublet a different Higgs doublet is needed:

$$\phi_c = -i\sigma_2\phi^* = \begin{pmatrix} -\bar{\phi}^0 \\ \phi^- \end{pmatrix}. \quad (2.51)$$

693 Additionally, given that the quark isospin doublets are not constructed in terms of
 694 the mass eigenstates but in terms of the flavor eigenstates as shown in table2.4, the
 695 coupling parameters will be related to the CKM matrix elements; thus the quark
 696 Lagrangian is given by:

$$\mathcal{L}_{Yq} = -G_d^{i,j}(\bar{u}_i, \bar{d}'_i)_L \begin{pmatrix} \phi^+ \\ \phi^0 \end{pmatrix} d_{jR} - G_u^{i,j}(\bar{u}_i, \bar{d}'_i)_L \begin{pmatrix} -\bar{\phi}^0 \\ \phi^- \end{pmatrix} u_{jR} + h.c. \quad (2.52)$$

697 with $i,j=1,2,3$. After SSB and expansion about the ground state, the diagonal form
 698 of \mathcal{L}_{Yq} is:

$$\mathcal{L}_{Yq} = -m_d^i \bar{d}_i d_i \left(1 + \frac{H}{v}\right) - m_u^i \bar{u}_i u_i \left(1 + \frac{H}{v}\right) \quad (2.53)$$

699 Fermion masses depends on arbitrary couplings G_l and $G_{u,d}$ and are not predicted
 700 by the theory.

701 2.3.5 The Higgs field

702 After the characterization of the fermions and gauge bosons as well as their inter-
 703 actions, it is necessary to characterize the Higgs field itself. The Lagrangian \mathcal{L}_S in
 704 eqn:2.37 written in terms of the gauge bosons is given by

$$\mathcal{L}_S = \frac{1}{4} \lambda v^4 + \mathcal{L}_H + \mathcal{L}_{HV} \quad (2.54)$$

$$705 \quad \mathcal{L}_H = \frac{1}{2} \partial_\mu H \partial^\mu H - \frac{1}{2} m_H^2 H^2 - \frac{1}{2v} m_H^2 H^3 - \frac{1}{8v^2} m_H^2 H^4 \quad (2.55)$$

$$706 \quad \mathcal{L}_{HV} = m_H^2 W_\mu^+ W^{\mu-} \left(1 + \frac{2}{v} H + \frac{2}{v^2} H^2\right) + \frac{1}{2} m_Z^2 Z_\mu Z^\mu \left(1 + \frac{2}{v} H + \frac{2}{v^2} H^2\right) \quad (2.56)$$

707 The mass of the Higgs boson is deduced as usual from the mass term in the Lagrangian
 708 resulting in:

$$m_H = \sqrt{-2\mu^2} = \sqrt{2\lambda}v \quad (2.57)$$

709 however, it too is not predicted by the theory. The experimental efforts to find the
 710 Higgs boson, carried out by the CMS and ATLAS experiments⁸, gave great results

⁸ CMS stands for Compact Muon Solenoid; ATLAS stand for A Toroidal LHC Apparatus. Both are general experiments held at the Large Hadron Collider(LHC)

711 by July of 2012 when the discovery of a new particles was announced and which
 712 is compatible with the Higgs boson predicted by the electroweak theory [39, 40].
 713 Although at the announcement time there were some reservations about calling the
 714 new particle the “Higgs boson”, today this name is widely accepted. The result of
 715 the measurement of the Higgs mass reported by both experiments [41] is in table 2.7.

Property	Value
Electric charge	0
Colour charge	0
Spin	0
Weak isospin	-1/2
Weak hypercharge	1
Parity	1
Mass (GeV/c^2)	$125.09 \pm 0.21 \text{ (stat.)} \pm 0.11 \text{ (syst.)}$

Table 2.7: Higgs boson properties. Higgs mass is not predicted by the theory and the value here corresponds to the experimental measurement.

716

717 2.3.6 Higgs boson production mechanisms at LHC.

718 At LHC, Higgs boson is produced as a result of the collision of two counter-rotating
 719 protons beams. A detailed description of the LHC machine will be presented in the
 720 chapter 3. “The total cross section” is the parameter that quantify the number of pp
 721 collisions that happen when a number of protons are fired at each other. Different
 722 results can be obtained after a pp collision and for each one the “cross section” is
 723 defined as the number of pp collisions that conclude in that particular result with
 724 respect to the number of protons fired at each other.

725 Protons are composed of quarks and these quarks are bound by gluons; however, what
 726 is commonly called the quark content of the proton makes reference to the valence
 727 quarks. A sea of quarks and gluons is also present inside the proton as represented
 728 in figure 2.10. In a proton-proton (pp) collision, the constituents (quarks and gluons)

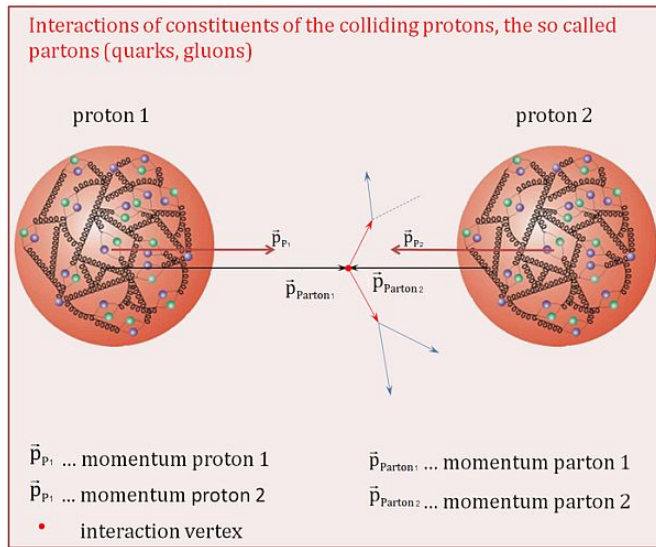


Figure 2.10: Proton-proton collision. Protons are composed of 3 valence quarks, a sea of quarks and gluons; therefore in a proton-proton collision, quarks and gluons are those who collide. [45].

are those who collide. The pp cross section depends on the momentum of the colliding particles, reason for which it is needed to know how the momentum is distributed inside the proton. Quarks and gluons are known as partons and the functions that describes how the proton momentum is distributed among partons inside it are called “parton distribution functions (PDFs)”; PDFs are determined from experimental data obtained in experiments where the internal structure of hadrons is tested.

In addition, in physics, a common approach to study complex systems consist in starting with a simpler version of them, for which a well known description is available, and add an additional “perturbation” which represent a small deviation from the known behavior. If the perturbation is small enough, the physical quantities associated with the perturbed system are expressed as a series of corrections to those of the simpler system; therefore, the more terms are considered in the series (the higher order in the perturbation series), the more precise is the the description of the complex system.

743 This thesis explore the Higgs production at LHC; therefore the overview presented
 744 here will be oriented specifically to the production mechanisms after pp collisions at
 745 LHC.

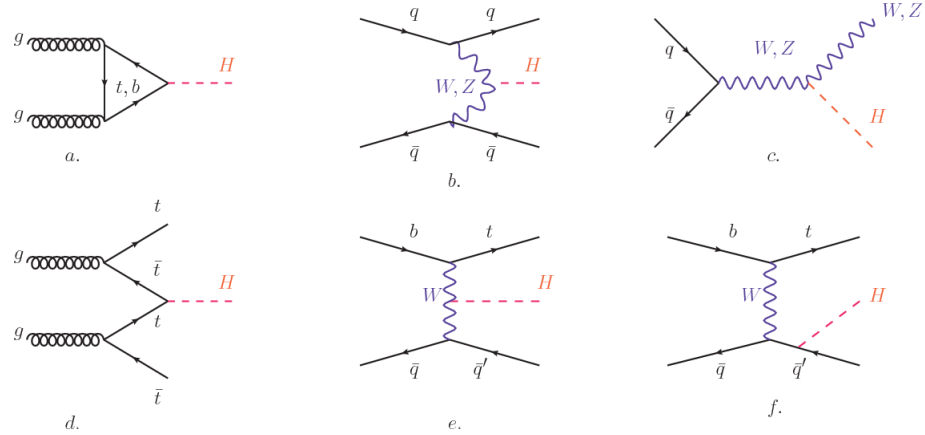


Figure 2.11: Main Higgs production mechanism Feynman diagrams. a. gluon-gluon fusion, b. vector boson fusion (VBF), c. Higgs-strahlung, d. Associated production with a top or bottom quark pair, e-f. associated production with a single top quark.

746 Figure 2.11 shows the Feynman diagrams for the leading order (first order) Higgs
 747 production processes at LHC, while the cross section for Higgs production as a func-
 748 tion of the center of mass-energy (\sqrt{s}) for pp collisions is showed in figure 2.12 left.
 749 The tags NLO (next to leading order), NNLO (next to next to leading order) and
 750 N3LO (next to next to next to leading order) make reference to the order at which
 751 the perturbation series has been considered.

752 As shown in eqns 2.48, 2.52 and 2.56, the strength of the Higgs-fermion interaction
 753 is proportional to the fermion mass while the strength of the Higgs-gauge boson
 754 interaction is proportional to the square of the gauge boson mass, which implies
 755 that the Higgs production and decay mechanisms are dominated by couplings $H -$
 756 (W, Z, t, b, τ) .

757 The main production mechanism is the gluon fusion (figure 2.11a and $pp \rightarrow H$ in figure
 758 2.12) given that gluons carry the highest fraction of momentum of the protons in pp

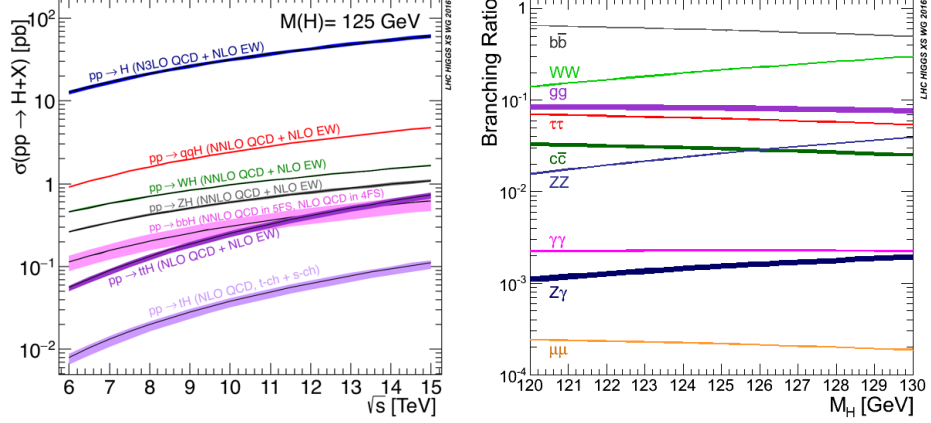


Figure 2.12: Higgs production cross sections (left) and decay branching ratios (right) for the main mechanisms. The VBF is indicated as qqH [42].

colliders. Since the Higgs boson does not couple to gluons, the mechanism proceeds through the exchange of a virtual top-quark loop given that for it the coupling is the biggest. Note that in this process, the Higgs boson is produced alone, which makes this mechanism experimentally clean when combined with the two-photon or the four-lepton decay channels (see section 2.3.7).

Vector boson fusion (figure 2.11b and $pp \rightarrow qqH$ in figure 2.12) has the second largest production cross section. The scattering of two fermions is mediated by a weak gauge boson which later emits a Higgs boson. In the final state, the two fermions tend to be located in a particular region of the detector which is used as a signature when analyzing the datasets provided by the experiments. More details about how to identify events of interest in an analysis will be given in chapter 4.

The next production mechanism is Higgs-strahlung (figure 2.11c and $pp \rightarrow WH, pp \rightarrow ZH$ in figure 2.12) where two fermions annihilate to form a weak gauge boson. If the initial fermions have enough energy, the emergent boson eventually will emit a Higgs boson.

The associated production with a top or bottom quark pair and the associated pro-

duction with a single top quark (figure 2.11d-f and $pp \rightarrow bbH, pp \rightarrow t\bar{t}H, pp \rightarrow tH$ in figure 2.12) have a smaller cross section than the main three mechanisms above, but they provide a good opportunity to test the Higgs-top coupling. The analysis reported in this thesis is developed using these production mechanisms. A detailed description of the tH mechanism will be given in section 2.4.

2.3.7 Higgs decay channels

When a particle can decays through several modes, also known as channels, the probability of decaying through a given channel is quantified by the “branching ratio (BR)” of the decay channel; thus, the BR is defined as the ratio of number of decays going through that given channel to the total number of decays. In regard to the Higgs boson decay, the BR can be predicted with accuracy once the Higgs mass is known [43, 44]. In figure 2.12 right, a plot of the BR as a function of the Higgs mass is presented. The largest predicted BR corresponds to the $b\bar{b}$ pair decay channel (see table 2.8).

Decay channel	Branching ratio	Rel. uncertainty
$H \rightarrow b\bar{b}$	5.84×10^{-1}	$+3.2\% - 3.3\%$
$H \rightarrow W^+W^-$	2.14×10^{-1}	$+4.3\% - 4.2\%$
$H \rightarrow \tau^+\tau^-$	6.27×10^{-2}	$+5.7\% - 5.7\%$
$H \rightarrow ZZ$	2.62×10^{-2}	$+4.3\% - 4.1\%$
$H \rightarrow \gamma\gamma$	2.27×10^{-3}	$+5.0\% - 4.9\%$
$H \rightarrow Z\gamma$	1.53×10^{-3}	$+9.0\% - 8.9\%$
$H \rightarrow \mu^+\mu^-$	2.18×10^{-4}	$+6.0\% - 5.9\%$

Table 2.8: Predicted branching ratios and the relative uncertainty for a SM Higgs boson with $m_H = 125\text{GeV}/c^2$. [21]

790 **2.4 Associated Production of Higgs Boson and**
 791 **Single Top Quark.**

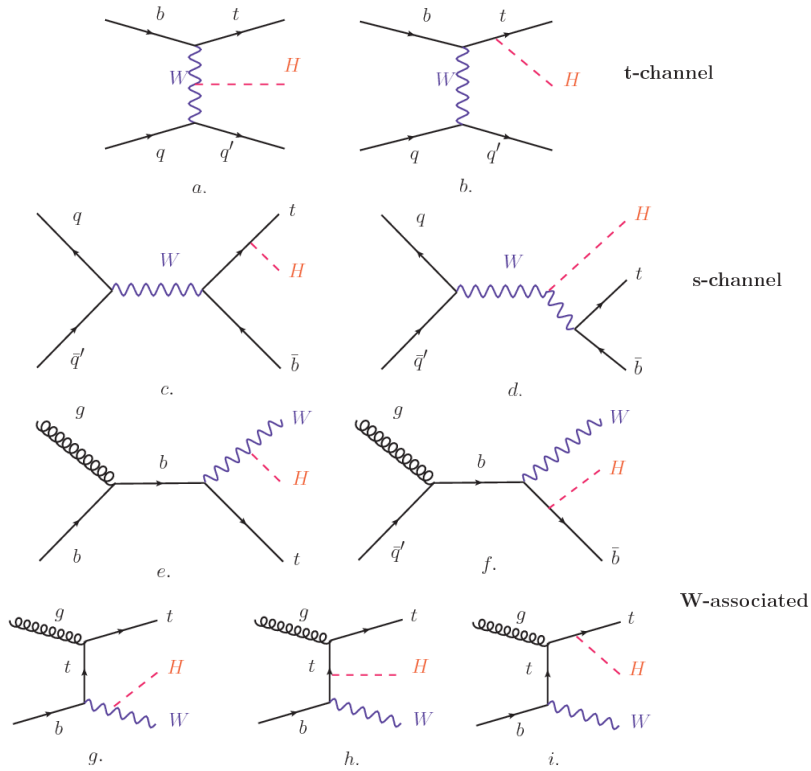


Figure 2.13: Associated higgs production mechanism Feynman diagrams. a.,b. t-channel (tHq), c.,d. s-channel (tHb), e-i. W-associated.

792 Associated production of Higgs boson have been extensively studied [46–50]. While
 793 measurements of the main Higgs production mechanisms rates are sensitive to the
 794 strength of the Higgs coupling to W boson or top quark, they are not sensitive to the
 795 relative sign between the two couplings. In this thesis, the Higgs boson production
 796 mechanism explored is the associated production with a single top quark (th) which
 797 offers sensitiveness to the relative sign of the Higgs couplings to W boson and to top
 798 quark. The description given here is based on the reference [48]

800 A process where two incoming particles interact and produce a final state with two
 801 particles can proceed in three ways also called channels (see, for instance, figure 2.13
 802 ommiting the red line). The t-channel represents processes where an intermediate
 803 particle is emitted by one of the incoming particles and absorbed by the other. The
 804 s-channel represent processes where the two incoming particles merge into an inter-
 805 mediate particle which eventually will split into the particles in the final state. The
 806 third channel, u-channel, is similar to the t-channel but the two outgoing particles
 807 interchange their roles.

808

809 The tH production where Higgs boson can be radiated either from the top quark or
 810 from the W boson is represented by the leading order Feynman diagrams in figure
 811 2.13. The cross section for the tH process is calculated, as usual, summing over
 812 the contributions from the different feynman diagrams; therefore it depends on the
 813 interference between the contributions. In the SM, the interference for t-channel (tHq
 814 process) and W-associated (tHW process) production is destructive [46] resulting in
 815 the small cross sections presented in table 2.9.

tH production channel	Cross section (fb)
t-channel ($pp \rightarrow tHq$)	$70.79^{+2.99}_{-4.80}$
W-associated ($pp \rightarrow tHW$)	$15.61^{+0.83}_{-1.04}$
s-channel($pp \rightarrow tHb$)	$2.87^{+0.09}_{-0.08}$

Table 2.9: Predicted SM cross sections for tH production at $\sqrt{s} = 13$ TeV [51, 52].

816

817 While the s-channel contribution can be neglected, it will be shown that a deviation
 818 from the SM destructive interference would result in an enhancement of the tH cross
 819 section compared to that in SM, which could be used to get information about the

820 sign of the Higgs-top coupling [48, 49]. In order to describe th production processes,
 821 Feynman diagram 2.13b will be considered; there, the W boson is radiated by a
 822 quark in the proton and eventually it will interact with the b quark. In the high
 823 energy regime, the effective W approximation [53] allows to describe the process as
 824 the emmision of an approximately on-shell W and its hard scattering with the b
 825 quark; i.e. $Wb \rightarrow th$. The scattering amplitude for the process is given by

$$\mathcal{A} = \frac{g}{\sqrt{2}} \left[(C_t - C_V) \frac{m_t \sqrt{s}}{m_W v} A \left(\frac{t}{s}, \varphi; \xi_t, \xi_b \right) + \left(C_V \frac{2m_W s}{v} \frac{1}{t} + (2C_t - C_V) \frac{m_t^2}{m_W v} \right) B \left(\frac{t}{s}, \varphi; \xi_t, \xi_b \right) \right], \quad (2.58)$$

826 where $C_V \equiv g_{HVV}/g_{HVV}^{SM}$ and $C_t \equiv g_{Ht}/g_{Ht}^{SM} = y_t/y_t^{SM}$ are scaling factors that quan-
 827 tify possible deviations of the couplings, Higgs-Vector boson (H-W) and Higgs-top
 828 (H-t) respectively, from the SM couplings; $s = (p_W + p_b)^2$, $t = (p_W - p_H)^2$, φ is the
 829 Higgs azimuthal angle around the z axis taken parallel to the direction of motion of
 830 the incoming W; A and B are funtions describing the weak interaction in terms of
 831 the chiral states of the quarks b and t. Terms that vanish in the high energy limit
 832 have been neglected as well as the Higgs and b quark masses⁹.

833 The scattering amplitude grows with energy like \sqrt{s} for $C_V \neq C_t$, in contract to
 834 the SM ($C_t = C_V = 1$) where the first term in 2.58 cancels out and the amplitude
 835 is constant for large s; therefore, a deviation from the SM predictions represent an
 836 enhancement in the tHq cross section. In particular, for a SM H-W coupling and
 837 a H-t coupling of inverted sigh with respect to the SM ($C_V = -C_t = 1$) the tHq
 838 cross section is enhanced by a factor greater 10 as seen in the figure 2.14 taken from
 839 reference [48]; reference [54] have reported similar enhancement results.
 840 A similar analysis is valid for the W-associated channel but, in that case, the inter-

⁹ A detailed explanation of the structure and approximations used to derive \mathcal{A} can be fount in reference [48]

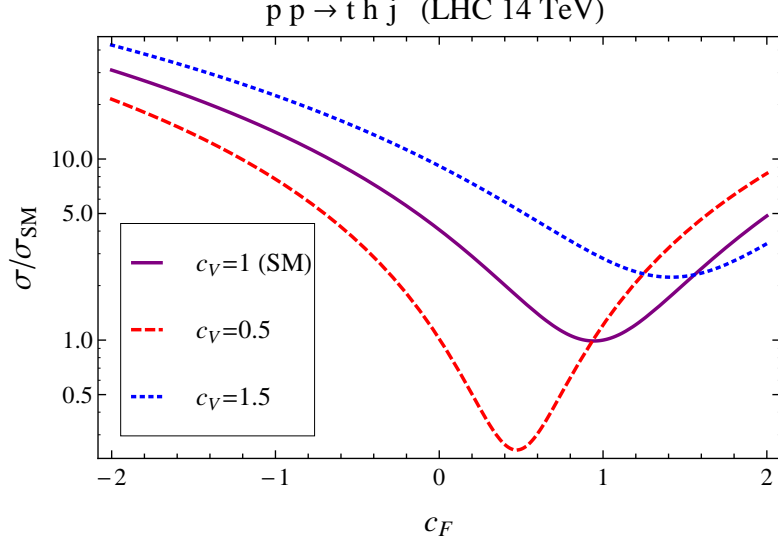


Figure 2.14: Cross section for tHq process as a function of C_t , normalized to the SM, for three values of C_V . In the plot C_f refers to the Higgs-fermion coupling which is dominated by the H-t coupling C_t . Solid, dashed and dotted lines correspond to $C_V = 1, 0.5, 1.5$ respectively. Note that for the SM ($C_V = C_t = 1$), the destructive effect of the interference is maximal.

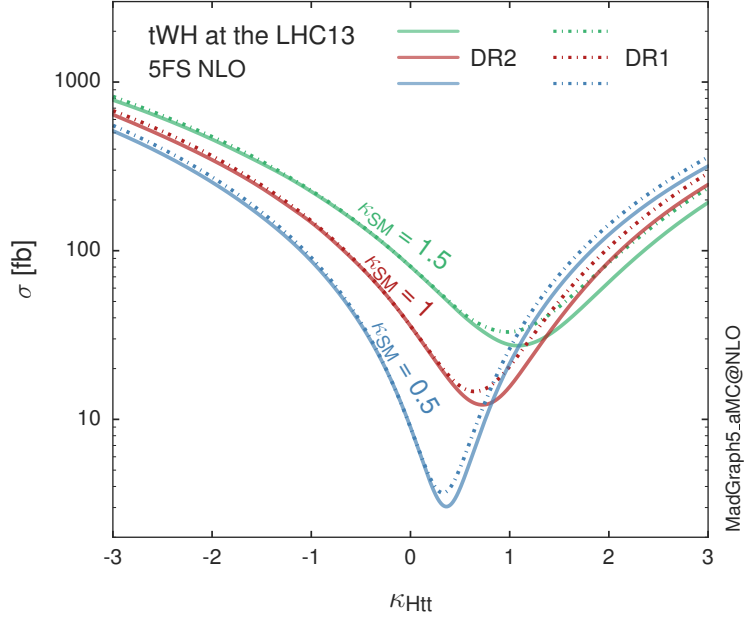


Figure 2.15: Cross section for tHW process as a function of κ_{Htt} , for three values of κ_{SM} at $\sqrt{s} = 13$ TeV. $\kappa_{Htt}^2 = \sigma_{Htt}/\sigma_{Htt}^{SM}$ is a simple rescaling of the SM Higgs interactions.

ference is more complicated since there are more than two contributions and an additional interference with the production of Higgs boson and a top pair process($t\bar{t}H$). The calculations are made using the so-called Diagram Removal (DR) technique where interfering diagrams are removed (or added) from the calculations in order to evaluate the impact of the removed contributions. DR1 was defined to neglect $t\bar{t}H$ interference while DR2 was defined to take $t\bar{t}H$ interference into account [55]. As shown in figure 2.15, the tHW cross section is enhanced from about 15 fb (SM: $\kappa_{Htt} = 1$) to about 150 fb ($\kappa_{Htt} = -1$). Differences between curves for DR1 and DR2 help to gauge the impact of the interference with $t\bar{t}H$. Results of the calculations of the tHq and tHW cross sections at $\sqrt{s} = 13$ TeV can be found in reference [56] and a summary of the results is presented in table 2.10.

	\sqrt{s} TeV	$C_t = 1$	$C_t = -1$
$\sigma^{LO}(tHq)(fb)$ [48]	8	≈ 17.4	≈ 252.7
	14	≈ 80.4	≈ 1042
$\sigma^{NLO}(tHq)(fb)$ [48]	8	$18.28^{+0.42}_{-0.38}$	$233.8^{+4.6}_{-0.0}$
	14	$88.2^{+1.7}_{-0.0}$	$982.8^{+28}_{-0.0}$
$\sigma^{LO}(tHq)(fb)$ [54]	14	≈ 71.8	≈ 893
$\sigma^{LO}(tHW)(fb)$ [54]	14	≈ 16.0	≈ 139
$\sigma^{NLO}(tHq)(fb)$ [56]	8	$18.69^{+8.62\%}_{-17.13\%}$	-
	13	$74.25^{+7.48\%}_{-15.35\%}$	$848^{+7.37\%}_{-13.70\%}$
	14	$90.10^{+7.34\%}_{-15.13\%}$	$1011^{+7.24\%}_{-13.39\%}$
$\sigma^{LO}(tHW)(fb)$ [55]	13	$15.77^{+15.91\%}_{-15.76\%}$	-
$\sigma^{NLO}DR1(tHW)(fb)$ [55]	13	$21.72^{+6.52\%}_{-5.24\%}$	≈ 150
$\sigma^{NLO}DR2(tHW)(fb)$ [55]	13	$16.28^{+7.34\%}_{-15.13\%}$	≈ 150

Table 2.10: Predicted enhancement of the tHq and tHW cross sections at LHC for $C_V = 1$ and $C_t = \pm 1$ at LO and NLO; the cross section enhancement of more than a factor of 10 is due to the flippling in the sign of the H-t coupling with respect to the SM one.

853 2.5 The CP-mixing in tH processes

854 In addition to the sensitivity to sign of the H-t coupling, tHq and tHW processes have
 855 been proposed as a tool to investigate the possibility of a H-t coupling that does not
 856 conserve CP [50, 55, 57]. Current experimental results are consistent with SM H-V
 857 and H-t couplings; however, negative H-t coupling is not excluded completely [60].

858

859 In this thesis, the sensitivity of th processes to CP-mixing is also studied in the
 860 effective field theory framework and based in references [50, 55]; a generic particle
 861 (X_0) of spin-0 and a general CP violating interaction with the top quark, can couples
 862 to scalar and pseudoscalar fermionic densities. The H-W interaction is assumed to
 863 be SM-like. The Lagrangian modeling the H-t interaction is given by

$$\mathcal{L}_0^t = -\bar{\psi}_t (c_\alpha \kappa_{Htt} g_{Htt} + i s_\alpha \kappa_{Att} g_{Att} \gamma_5) \psi_t X_0, \quad (2.59)$$

864 where α is the CP-mixing phase, $c_\alpha \equiv \cos \alpha$ and $s_\alpha \equiv \sin \alpha$, κ_{Htt} and κ_{Att} are real
 865 dimensionless rescaling parameters¹⁰, $g_{Htt} = g_{Att} = m_t/v = y_t/\sqrt{2}$ and $v \sim 246$ GeV
 866 is the Higgs vacuum expectation value. In this parametrization, it is easy to recover
 867 three special cases

868 • CP-even coupling $\rightarrow \alpha = 0^\circ$

869 • CP-odd coupling $\rightarrow \alpha = 90^\circ$

870 • SM coupling $\rightarrow \alpha = 0^\circ$ and $\kappa_{Htt} = 1$

871 The loop induced X_0 coupling to gluons can also be described in terms of the
 872 parametrization above, according to

¹⁰ analog to C_t and C_V

$$\mathcal{L}_0^g = -\frac{1}{4} \left(c_\alpha \kappa_{Hgg} g_{Hgg} G_{\mu\nu}^a G^{a,\mu\nu} + s_\alpha \kappa_{Agg} g_{Agg} G_{\mu\nu}^a \tilde{G}^{a,\mu\nu} \right) X_0. \quad (2.60)$$

873 where $g_{Hgg} = -\alpha_s/3\pi v$ and $g_{Agg} = \alpha_s/2\pi v$. Under the assumption that the top quark
 874 dominates the gluon-fusion process at LHC energies, $\kappa_{Hgg} \rightarrow \kappa_{Htt}$ and $\kappa_{Agg} \rightarrow \kappa_{Att}$,
 875 so that the ratio between the gluon-gluon fusion cross section for X_0 and for the SM
 876 Higgs prediction can be written as

$$\frac{\sigma_{NLO}^{gg \rightarrow X_0}}{\sigma_{NLO,SM}^{gg \rightarrow H}} = c_\alpha^2 \kappa_{Htt}^2 + s_\alpha^2 \left(\kappa_{Att} \frac{g_{Agg}}{g_{Hgg}} \right)^2. \quad (2.61)$$

877 If the rescaling parameters are set to

$$\kappa_{Htt} = 1, \quad \kappa_{Att} = \left| \frac{g_{Hgg}}{g_{Agg}} \right| = \frac{2}{3}. \quad (2.62)$$

878 the gluon-fusion SM cross section is reproduced for every value of the CP-mixing
 879 angle α ; therefore, by imposing that condition to the Lagrangian density 2.59, the
 880 CP-mixing angle is not constrained by current data. Figure 2.16 shows the NLO cross
 881 sections for t-channel tX_0 (blue) and $t\bar{t}X_0$ (red) associated production processes as
 882 a function of the CP-mixing angle α . X_0 is a generic spin-0 particle with top quark
 883 CP-violating coupling. Rescaling factors κ_{Htt} and κ_{Att} have been set to reproduce
 884 the SM gluon-fusion cross sections.

885 It is interesting to notice that the tX_0 cross section is enhanced, by a factor of
 886 about 10, when a continuous rotation in the scalar-pseudoscalar plane is applied; this
 887 enhancement is similar to the enhancement produced when the H-t coupling is flipped
 888 in sign with respect to the SM ($y_t = -y_{t,SM}$ in the plot), as showed in section 2.4. In
 889 contrast, the degeneracy in the $t\bar{t}X_0$ cross section is still present given that it depends
 890 quadratically on the H-t coupling, but more interesting is to notice that $t\bar{t}X_0$ cross

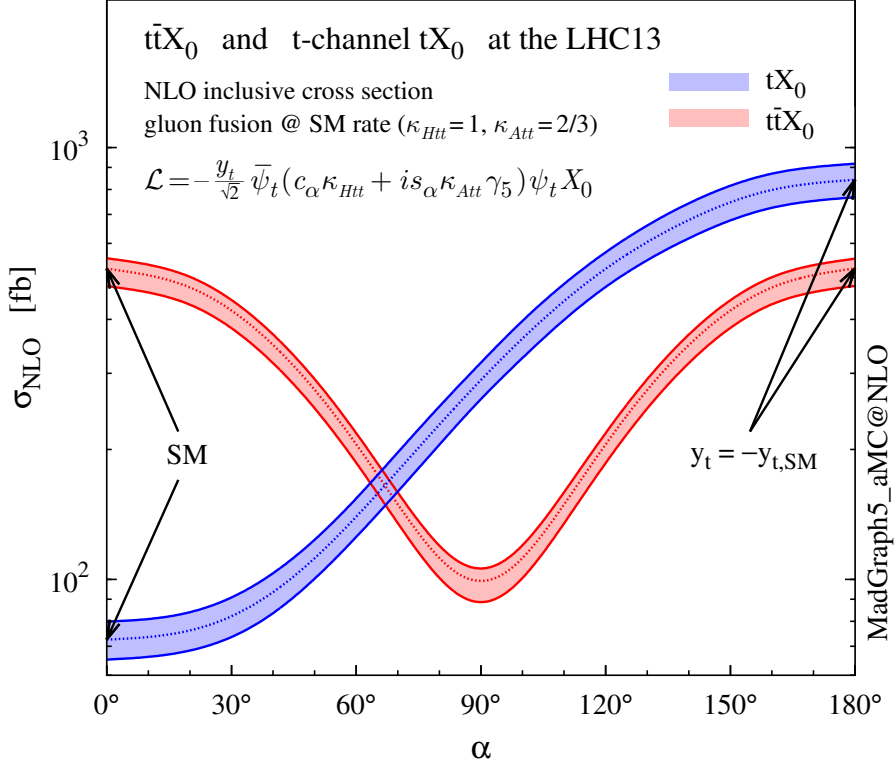


Figure 2.16: NLO cross sections for t-channel tX_0 (blue) and $t\bar{t}X_0$ (red) associated production processses as a function of the CP-mixing angle α . X_0 is a generic spin-0 particle with top quark CP-violating coupling [50].

891 section is exceeded by tX_0 cross section after $\alpha \sim 60^\circ$.

892 A similar parametrization can be used to investigate the tHW process sensitivity to
 893 CP-violating H-t coupling. As said in 2.4, the interference in the W-associated channel
 894 is more complicated because there are more than two contributions and also there is
 895 interference with the $t\bar{t}H$ production process.

896 Figure 2.17 shows the NLO cross sections for t-channel tX_0 (blue), $t\bar{t}X_0$ (red) asso-
 897 ciated production and for the combined $tWX_0 + t\bar{t}X_0 +$ interference (orange) as a
 898 function of the CP-mixing angle. It is clear that the effect of the interference in the
 899 combined case is the lifting of the degeneracy present in the $t\bar{t}X_0$ production. The
 900 constructive interference enhance the cross section from about 500 fb at $\alpha = 0$

to about 600 fb ($\alpha = 180^\circ \rightarrow y_t = -y_{t,SM}$).

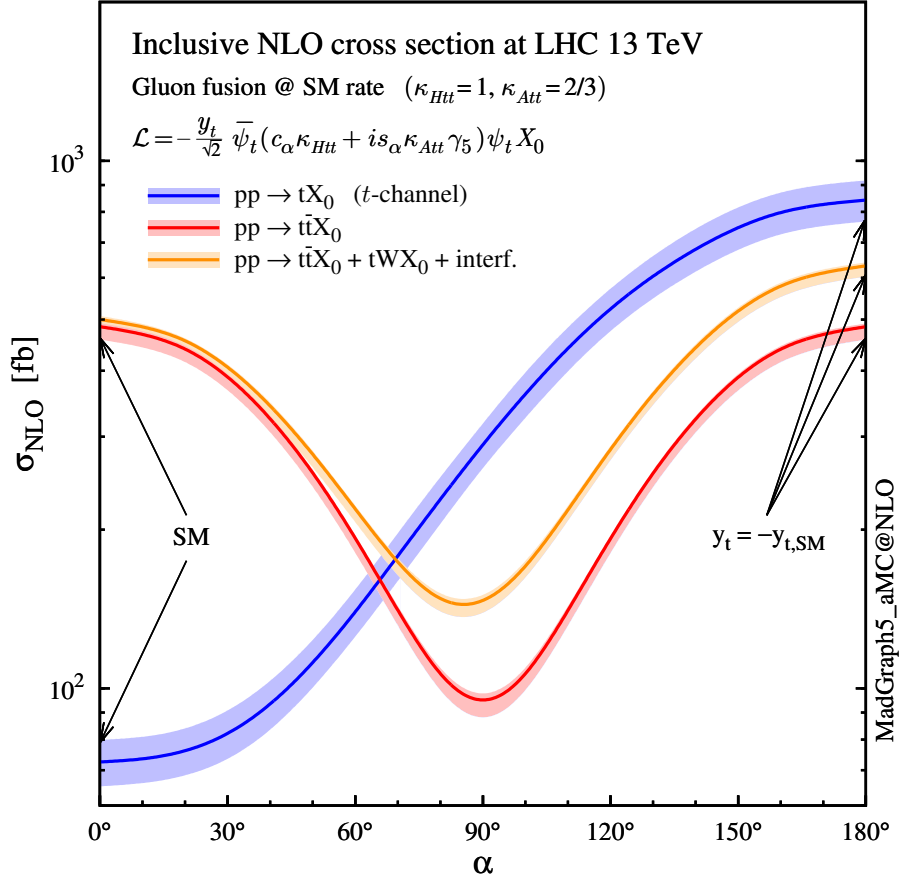


Figure 2.17: NLO cross sections for t-channel tX_0 (blue), $t\bar{t}X_0$ (red) associated production processses and combined $tWX_0 + t\bar{t}X_0$ (including interference) production as a function of the CP-mixing angle α [50].

901

902 An analysis combining tHq and tHW proceses will be made in this thesis taking
 903 advantage of the sensitivity improvement.

904 **Chapter 3**

905 **The CMS experiment at the LHC**

906 **3.1 Introduction**

907 Located in the Swiss-French border, the European Council for Nuclear Research
908 (CERN) is the largest scientific organization leading the particle physics research.
909 About 13000 people in a broad range of fields including users, students, scientists,
910 engineers among others, contribute to the data taking and analysis, with the goal
911 of unveiling the secrets of the nature and revealing the fundamental structure of the
912 universe. CERN is also the home of the Large Hadron Collider (LHC), the largest
913 circular particle accelerator around the world, where protons (or heavy ions) traveling
914 close to the speed of light, are made to collide. These collisions open a window to
915 investigate how particles (and their constituents if they are composite) interact with
916 each other, providing clues about the laws of the nature.

917 LHC can run in three modes depending on the particles being accelerated

918 • Proton-Proton collisions (pp) multiple physics experiments .

919 • Lead-Lead collisions (Pb-Pb) Heavy ion experiments.

920 • Proton-Lead collisions (p-Pb).

921 Figure 3.1 show an overview of the CERN accelerating complex. There are several
 922 accelerating stages before the injection to the LHC ring. In the pp mode, after
 923 removing the electrons from hydrogen atoms in a bottle, protons are accelerated
 924 in the LINAC2 to 50 MeV and then injected into the proton synchrotron booster
 925 (BOOSTER) to reach 1.4 GeV in energy. The next boost is provided at the proton
 926 synchrotron (PS) up to 26 GeV, followed by the injection into the super proton
 927 synchrotron (SPS) where protons are accelerated to 450 GeV. Finally, protons are
 928 injected into the LHC where they are accelerated to the target energy of 6.5 TeV. In
 929 the Pb-Pb mode, the Lead ions are first accelerated in the LINAC3 and then passed as
 930 long pulses to the Low energy ion ring (LEIR) to be converted into short and dense
 931 bunches, each containing 7×10^7 lead ions. LEIR accelerate the bunches from 4.2
 932 MeV to 72 MeV. The ions are then passed to the PS to follow the rest of acceleration
 933 process up to 2.8TeV/n en the LHC ring.

934 3.2 The LHC

935 The LHC is a 27 km ring composed of superconducting magnets and accelerating
 936 structures (among other components) which boost the particles traveling inside it.
 937 It is installed in the same tunnel where the large Electron-Positron (LEP) collider
 938 was located, taking advantage of the existing infraestructure as shown in Figure 3.2.
 939 Two particle beams travel counter-rotating in two separated beam pipes kept at ultra
 940 high vacuum. In 2008, the first set of collisions involved protons with center-of-mass
 941 energy of 7 TeV after which the energy was increased to 8 TeV in 2012 and to 13 TeV
 942 in 2015.

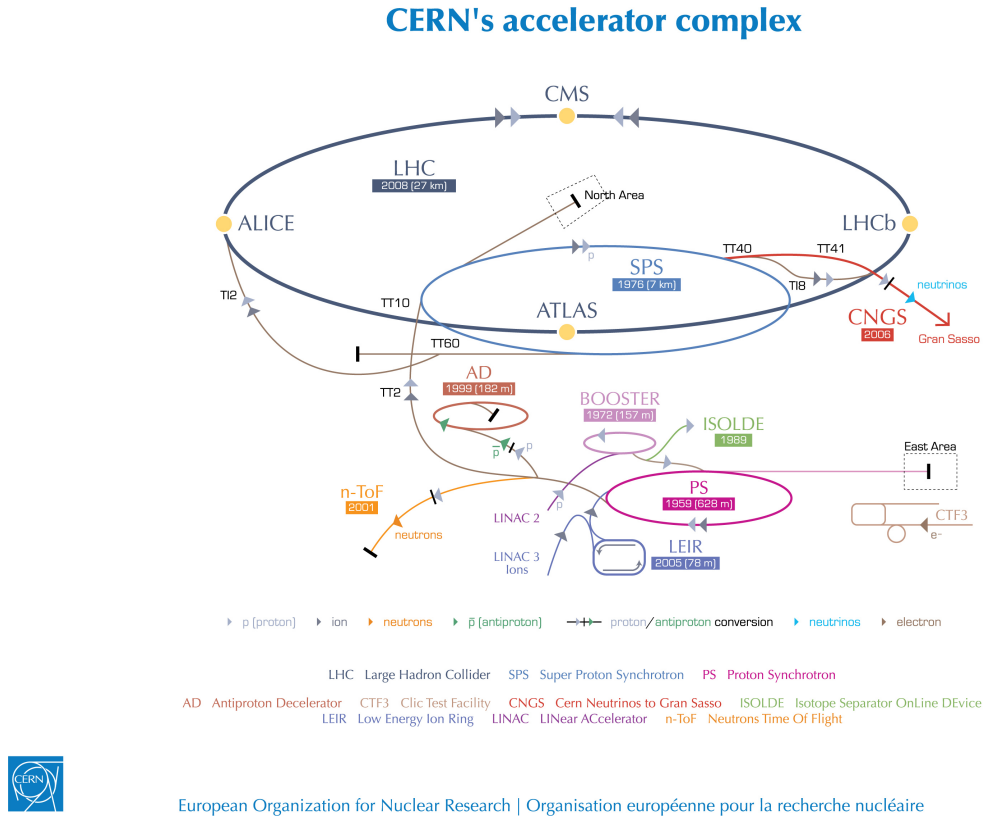
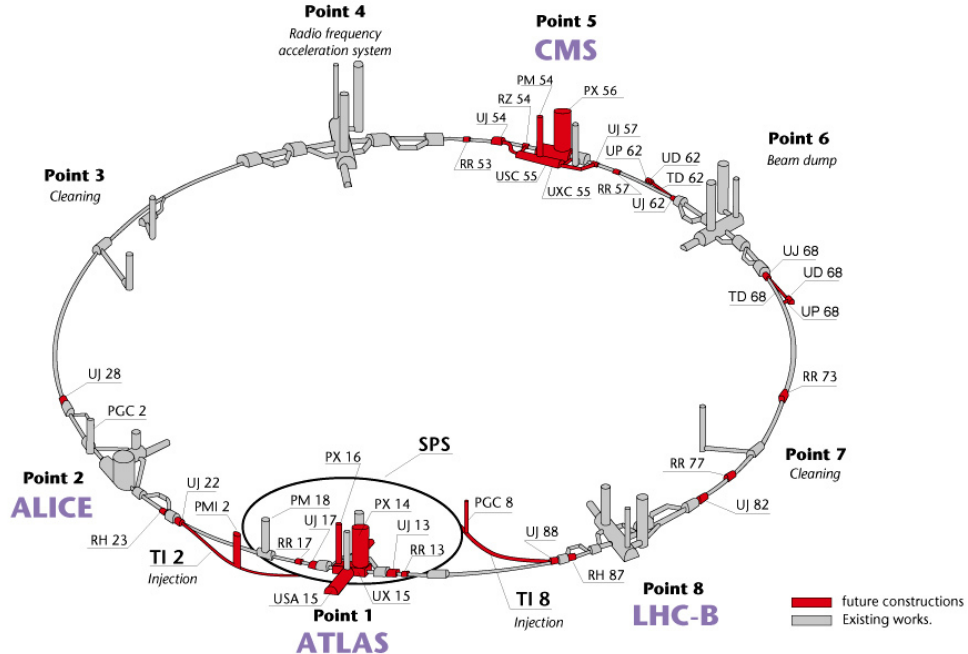


Figure 3.1: ref. C.Lefevre, “The CERN accelerator complex,” (2008). CERN-DI-0812015.

943 In order to keep the protons in the circular trajectory carrying that amount of
 944 energy, strong magnetic fields are needed, bringing the superconductivity into scene.
 945 The superconducting dipole magnets used in LHC are made of a NbTi alloy, capable
 946 of transporting currents of about 12000 A when cooled at a temperature below 2K by
 947 using liquid helium; that current generates a magnetic fields of 8.3 T. Figure 3.3 shows
 948 the transverse view of the LHC dipole magnets. Additionally, quadrupole magnets
 949 are used to focus the beam and some other magnetic multipoles are used to correct
 950 effects generated by the interaction among protons in the beam as well as interactions
 951 within the beam pipe.
 952 Regarding to the longitudinal acceleration of the protons, a system of 16 radio-
 953 frecuency cavities (RF) (8 per beam) is used to accelerate protons. Inside the cavities,

Layout of the LEP tunnel including future LHC infrastructures.



CERN AC _ hf238 _ V02/02/98

Figure 3.2: ref. J.-L. Caron , “Layout of the LEP tunnel including future LHC infrastructures.. L’ensemble du tunnel LEP avec les futures infrastructures LHC.”, <https://cds.cern.ch/record/841542> (Nov, 1993). AC Collection. Legacy of AC. Pictures from 1992 to 2002..

954 the electromagnetic waves become resonant transferring the maximum energy to the
 955 particle flight through it. Cavities are cooled at 4.5 K. On LHC the RF oscillation
 956 frecuency is 400MHz and the protons are carefully timed so additionally to the ac-
 957 celeration effect the bunch structure of the beam is preserved. The Beam is made
 958 of 2808 “bunches” which are packages of 1.15×10^{11} protons ???. If LHC is at full
 959 energy, protons with the right energy does not feel any accelerating force but those
 960 with a different energy will be accelerated or decelerated to keep them in the bunch.
 961 The paths followed by particles during the acceleration process are shown in Figure
 962 3.1.

LHC DIPOLE : STANDARD CROSS-SECTION

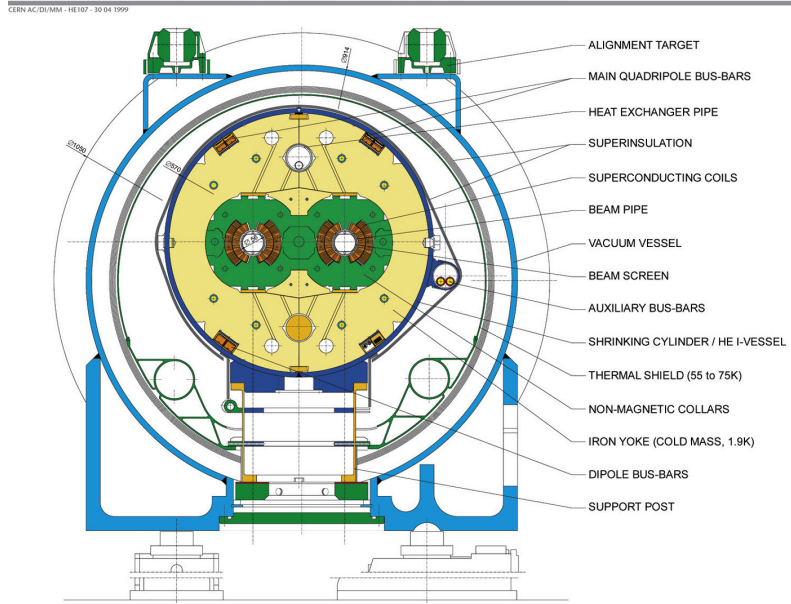


Figure 3.3: ref. ACTeam, “Diagram of an LHC dipole magnet. Schéma d’un aimant dipôle du LHC,” (1999). CERN-DI-9906025.

963 Once the beams reach the desired energy, they are brought to cross each other
 964 producing proton-proton collisions. The bunch crossing happens in precise places
 965 where the LHC experiments are located. As seen in Figure 3.2, it was needed to
 966 build the caverns for CMS and ATLAS as well as some additional facilities, but
 967 most of the initial LEP infrastructure has been used to allocate additional collision
 968 points. The highest luminosity is delivered at the CMS (point 5) and ATLAS (point
 969 1) experiments, which are general purpose experiments, enabled to explore physics
 970 in any of the collision modes. LHCb (point 8) experiment is optimized to explore
 971 B-physics, while ALICE (point 2) is optimized for heavy ion collisions researches;
 972 TOTEM (point 5) and LHCf (point 1) are dedicated to forward physics studies and
 973 MoEDAL (point 8) is intended for monopoles or massive pseudo stable particles
 974 studies.

975 3.3 The CMS experiment

976 The Compact Muon Solenoid (CMS) is a general purpose detector designed to conduct
977 research in a wide range of physics from standard model to new physics like extra
978 dimensions and dark matter. Located at the point 5 in the LHC layout as shown in
979 Figure 3.2, CMS is composed by several detection systems distributed in a cylindrical
980 structure where the main feature is a solenoid magnet made of superconducting cable
981 capable to generate a 3.8 T magnetic field. In total, CMS weight about 14000 tons
982 in a very compact 21.6 m long and 14.6 m diameter cylinder (include areference for
983 CMS TDR). It was built in 15 separated sections at the ground level and lowered
984 to the cavern individually to be assembled. Figure 3.4 show the layout of the CMS
985 detector (CMS TDR).

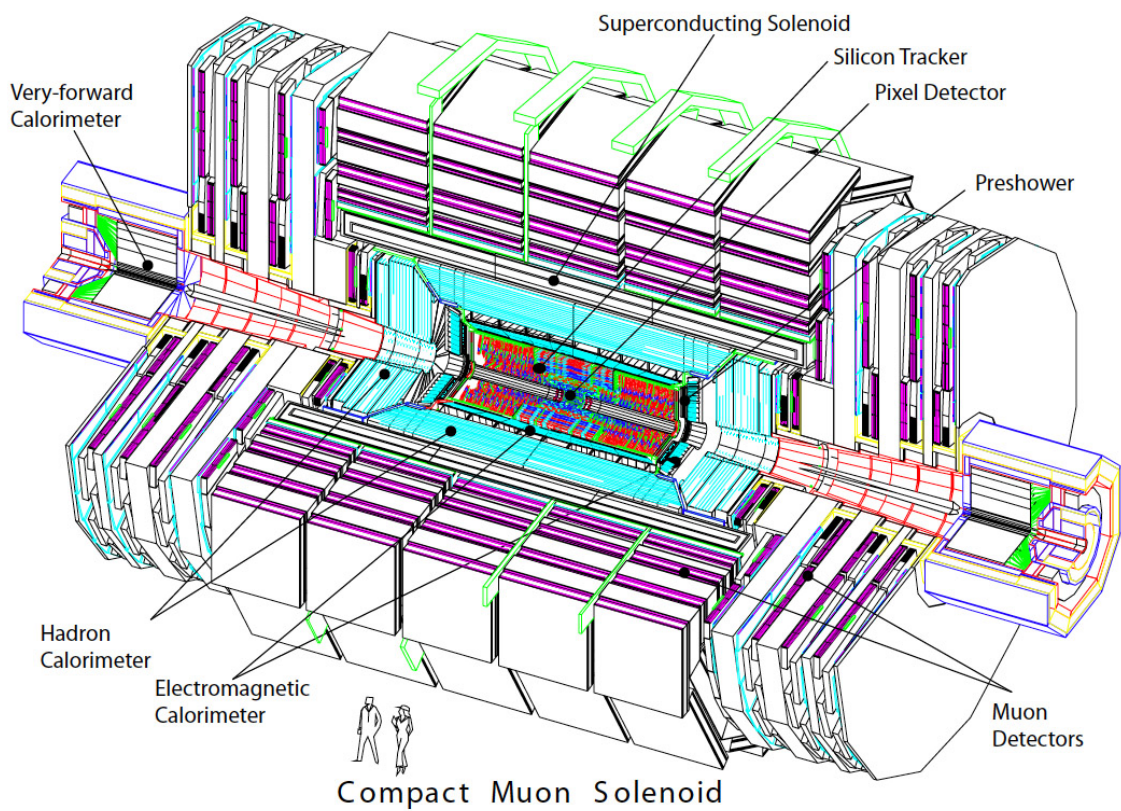


Figure 3.4: ref: CMS Collaboration, “Detector Drawings”, CMS-PHO-GEN-2012-002, <http://cds.cern.ch/record/1433717>, 2012.

⁹⁸⁶ Chapter 4

⁹⁸⁷ **Search for production of a Higgs**
⁹⁸⁸ **boson and a single top quark in**
⁹⁸⁹ **multilepton final states in pp**
⁹⁹⁰ **collisions at $\sqrt{s} = 13$ TeV**

⁹⁹¹ 4.1 Introduction

⁹⁹² Dont forget to mention previous constrains to ct check reference ?? and references
⁹⁹³ <https://link.springer.com/content/pdf/10.1007%2FJHEP01>
⁹⁹⁴ A. Azatov, R. Contino and J. Galloway, â€œModel-Independent Bounds on a
⁹⁹⁵ Light Higgs,â€ JHEP 1204 (2012) 127 [arXiv:1202.3415 [hep-ph]].
⁹⁹⁶ J. R. Espinosa, C. Grojean, M. Muhlleitner and M. Trott, â€œFingerprinting
⁹⁹⁷ Higgs Suspects at the LHC,â€ JHEP 1205 (2012) 097 [arXiv:1202.3697 [hep-ph]].
⁹⁹⁸ This chapter present the search for the associated production of a Higgs boson and
⁹⁹⁹ a single top quark events with three leptons in the final state, targeting Higgs decay

1000 modes to WW , ZZ , and $\tau\tau$. The analysis uses the 13 TeV dataset produced in 2016,
 1001 corresponding to an integrated luminosity of 35.9fb^{-1} . It is based on and expands
 1002 previous analyses at 8 TeV [61, 62] and searches for associated production of $t\bar{t}$ and
 1003 Higgs in the same channel [63], and complements searches in other decay channels
 1004 targeting $H \rightarrow b\bar{b}$ [64].

1005 As showed in section 2.4, the cross section of the associated production of a Higgs
 1006 boson and a single top quark (tHq) process is driven by a destructive interference of
 1007 two contributions (see Figure 4.1), where the Higgs couples to either the W boson or
 1008 the top quark. Any deviation from the standard model (SM) in the Higgs coupling
 1009 structure could therefore lead to a large enhancement of the cross section, making
 1010 this analysis sensitive to such deviations. A second process, where the Higgs and
 1011 top quark are accompanied by a W boson (tHW) has similar behavior, albeit with a
 1012 weaker interference pattern.

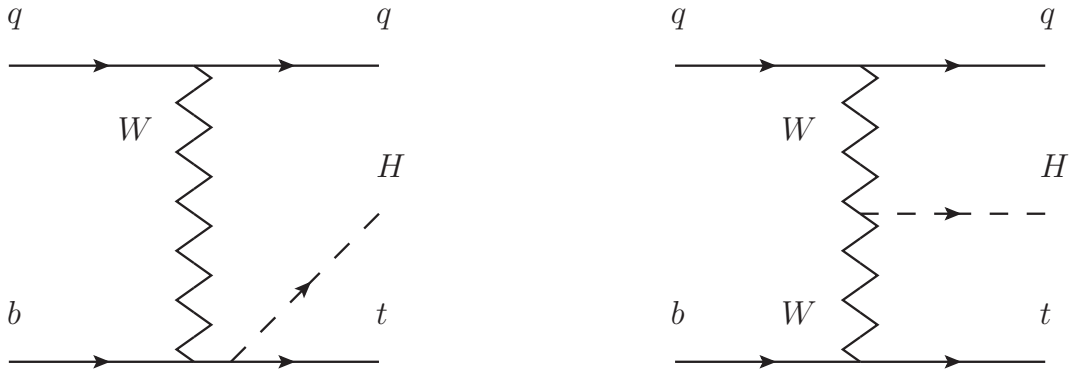


Figure 4.1: The two leading-order diagrams of tHq production.

1013 We selects events with three leptons and a b tagged jet in the final state. The tHq
 1014 signal contribution is then determined in a fit of the observed data to two multivariate
 1015 classifier outputs, each trained to discriminate against one of the two dominant back-
 1016 grounds of events with non-prompt leptons from $t\bar{t}$ and of associated production of $t\bar{t}$

1017 and vector bosons ($t\bar{t}W$, $t\bar{t}Z$). The fit result is then used to set an upper limit on the
 1018 combined $t\bar{t}H$, tHq and tHW production cross section, as a function of the relative
 1019 coupling strengths of Higgs and top quark and Higgs and W boson, respectively.

1020 4.2 Data and MC Samples

1021 The data considered in this analysis were collected by the CMS experiment dur-
 1022 ing 2016 and correspond to a total integrated luminosity of 35.9fb^{-1} . Only periods
 1023 when the CMS magnet was on were considered when selecting the data samples, that
 1024 corresponds to the 23 Sep 2016 (Run B to G) and PromptReco (Run H) versions
 1025 of the datasets. The MC samples used in this analysis correspond to the RunI-
 1026 ISummer16MiniAODv2 campaign produced with CMSSW 80X. The two signal sam-
 1027 ples (for tHq and tHW) were produced with MG5_aMC@NLO (version 5.222), in
 1028 leading-order mode, and are normalized to next-to-leading-order cross sections,
 1029 see Tab. 4.1. Each sample is generated with a set of event weights corresponding to
 1030 different values of κ_t and κ_V couplings as shown in Tab. 4.2.

1031 4.2.1 Full 2016 dataset and MC samples

Sample	σ [pb]	BF
/THQ_Hincl_13TeV-madgraph-pythia8_TuneCUETP8M1/	0.7927	0.324
/THW_Hincl_13TeV-madgraph-pythia8_TuneCUETP8M1/	0.1472	1.0

Table 4.1: Signal samples and their cross section and branching fraction used in this analysis. See Ref. [65] for more details.

1032 Different MC generators were used to generate the background processes. The
 1033 dominant sources ($t\bar{t}$, $t\bar{t}W$, $t\bar{t}Z$, $t\bar{t}H$) were produced using AMC@NLO interfaced
 1034 to PYTHIA8, and are scaled to NLO cross sections. Other processes are simulated

		<i>tHq</i>		<i>tHW</i>		
κ_V	κ_t	sum of weights	cross section [pb]	sum of weights	cross section [pb]	LHE weights
1.0	-3.0	35.700022	2.991	11.030445	0.6409	LHEweight_wgt[446]
1.0	-2.0	20.124298	1.706	5.967205	0.3458	LHEweight_wgt[447]
1.0	-1.5	14.043198	1.205	4.029093	0.2353	LHEweight_wgt[448]
1.0	-1.25	11.429338	0.9869	3.208415	0.1876	LHEweight_wgt[449]
1.0	-1.0		0.7927		0.1472	
1.0	-0.75	7.054998	0.6212	1.863811	0.1102	LHEweight_wgt[450]
1.0	-0.5	5.294518	0.4723	1.339886	0.07979	LHEweight_wgt[451]
1.0	-0.25	3.818499	0.3505	0.914880	0.05518	LHEweight_wgt[452]
1.0	0.0	2.627360	0.2482	0.588902	0.03881	LHEweight_wgt[453]
1.0	0.25	1.719841	0.1694	0.361621	0.02226	LHEweight_wgt[454]
1.0	0.5	1.097202	0.1133	0.233368	0.01444	LHEweight_wgt[455]
1.0	0.75	0.759024	0.08059	0.204034	0.01222	LHEweight_wgt[456]
1.0	1.0	0.705305	0.07096	0.273617	0.01561	LHEweight_wgt[457]
1.0	1.25	0.936047	0.0839	0.442119	0.02481	LHEweight_wgt[458]
1.0	1.5	1.451249	0.1199	0.709538	0.03935	LHEweight_wgt[459]
1.0	2.0	3.335034	0.2602	1.541132	0.08605	LHEweight_wgt[460]
1.0	3.0	10.516125	0.8210	4.391335	0.2465	LHEweight_wgt[461]
<hr/>						
1.5	-3.0	45.281492	3.845	13.426212	0.7825	LHEweight_wgt[462]
1.5	-2.0	27.606715	2.371	7.809713	0.4574	LHEweight_wgt[463]
1.5	-1.5	20.476088	1.784	5.594971	0.3290	LHEweight_wgt[464]
1.5	-1.25	17.337465	1.518	4.635978	0.2749	LHEweight_wgt[465]
1.5	-1.0	14.483302	1.287	3.775902	0.2244	LHEweight_wgt[466]
1.5	-0.75	11.913599	1.067	3.014744	0.1799	LHEweight_wgt[467]
1.5	-0.5	9.628357	0.874	2.352505	0.1410	LHEweight_wgt[468]
1.5	-0.25	7.627574	0.702	1.789184	0.1081	LHEweight_wgt[469]
1.5	0.0	5.911882	0.5577	1.324946	0.08056	LHEweight_wgt[470]
1.5	0.25	4.479390	0.4365	0.959295	0.05893	LHEweight_wgt[471]
1.5	0.5	3.331988	0.3343	0.692727	0.04277	LHEweight_wgt[472]
1.5	0.75	2.469046	0.2558	0.525078	0.03263	LHEweight_wgt[473]
1.5	1.0	1.890565	0.2003	0.456347	0.02768	LHEweight_wgt[474]
1.5	1.25	1.596544	0.1689	0.486534	0.02864	LHEweight_wgt[475]
1.5	1.5	1.586983	0.1594	0.615638	0.03509	LHEweight_wgt[476]
1.5	2.0	2.421241	0.2105	1.170602	0.06515	LHEweight_wgt[477]
1.5	3.0	7.503280	0.5889	3.467546	0.1930	LHEweight_wgt[478]
<hr/>						
0.5	-3.0	27.432685	2.260	8.929074	0.5136	LHEweight_wgt[479]
0.5	-2.0	13.956013	1.160	4.419093	0.2547	LHEweight_wgt[480]
0.5	-1.5	8.924438	0.7478	2.757611	0.1591	LHEweight_wgt[481]
0.5	-1.25	6.835341	0.5726	2.075247	0.1204	LHEweight_wgt[482]
0.5	-1.0	5.030704	0.4273	1.491801	0.08696	LHEweight_wgt[483]
0.5	-0.75	3.510528	0.2999	1.007273	0.05885	LHEweight_wgt[484]
0.5	-0.5	2.274811	0.1982	0.621663	0.03658	LHEweight_wgt[485]
0.5	-0.25	1.323555	0.1189	0.334972	0.01996	LHEweight_wgt[486]
0.5	0.0	0.656969	0.06223	0.147253	0.008986	LHEweight_wgt[487]
0.5	0.25	0.274423	0.02830	0.058342	0.003608	LHEweight_wgt[488]
0.5	0.5	0.176548	0.01778	0.068404	0.003902	LHEweight_wgt[489]
0.5	0.75	0.363132	0.03008	0.177385	0.009854	LHEweight_wgt[490]
0.5	1.0	0.834177	0.06550	0.385283	0.02145	LHEweight_wgt[491]
0.5	1.25	1.589682	0.1241	0.692099	0.03848	LHEweight_wgt[492]
0.5	1.5	2.629647	0.2047	1.097834	0.06136	LHEweight_wgt[493]
0.5	2.0	5.562958	0.4358	2.206057	0.1246	LHEweight_wgt[494]
0.5	3.0	14.843102	1.177	5.609519	0.3172	LHEweight_wgt[495]

Table 4.2: κ_V and κ_t combinations generated for the two signal samples and their NLO cross sections. The *tHq* cross section is multiplied by the branching fraction of the enforced leptonic decay of the top quark (0.324). See also Ref. [65].

Sample	σ [pb]
TTWJetsToLNu_TuneCUETP8M1_13TeV-amcatnloFXFX-madspin-pythia8	0.2043
TTZToLLNuNu_M-10_TuneCUETP8M1_13TeV-amcatnlo-pythia8	0.2529
ttHJetToNonbb_M125_13TeV_amcatnloFXFX_madspin_pythia8_mWCutfix	0.2151
/store/cmst3/group/susy/gpetrucc/13TeV/u/TTLL_m1to10_LO_NoMS_for76X/	0.0283
WGToLNug_TuneCUETP8M1_13TeV-madgraphMLM-pythia8	585.8
ZGTo2LG_TuneCUETP8M1_13TeV-amcatnloFXFX-pythia8	131.3
TGJets_TuneCUETP8M1_13TeV_amcatnlo_madspin_pythia8	2.967
TGJets_TuneCUETP8M1_13TeV_amcatnlo_madspin_pythia8	2.967
TTGJets_TuneCUETP8M1_13TeV-amcatnloFXFX-madspin-pythia8	3.697
WpWpJJ_EWK-QCD_TuneCUETP8M1_13TeV-madgraph-pythia8	0.03711
ZZZ_TuneCUETP8M1_13TeV-amcatnlo-pythia8	0.01398
WWZ_TuneCUETP8M1_13TeV-amcatnlo-pythia8	0.1651
WZZ_TuneCUETP8M1_13TeV-amcatnlo-pythia8	0.05565
WW_DoubleScattering_13TeV-pythia8	1.64
tZq_1l_4f_13TeV-amcatnlo-pythia8_TuneCUETP8M1	0.0758
ST_tW1l_5f_L0_13TeV-MadGraph-pythia8	0.01123
TTTT_TuneCUETP8M1_13TeV-amcatnlo-pythia8	0.009103
WZTo3LNu_TuneCUETP8M1_13TeV-powheg-pythia8	4.4296
ZZTo4L_13TeV_powheg_pythia8	1.256
TTJets_SingleLeptFromTbar_TuneCUETP8M1_13TeV-madgraphMLM-pythia8	182.1754
TTJets_SingleLeptFromT_TuneCUETP8M1_13TeV-madgraphMLM-pythia8	182.1754
TTJets_DiLept_TuneCUETP8M1_13TeV-madgraphMLM-pythia8	87.3
DYJetsToLL_M-10to50_TuneCUETP8M1_13TeV-amcatnloFXFX-pythia8	18610
DYJetsToLL_M-50_TuneCUETP8M1_13TeV-madgraphMLM-pythia8	6024
WJetsToLNu_TuneCUETP8M1_13TeV-amcatnloFXFX-pythia8	61526.7
ST_tW_top_5f_inclusiveDecays_13TeV-powheg-pythia8_TuneCUETP8M1	35.6
ST_tW_antitop_5f_inclusiveDecays_13TeV-powheg-pythia8_TuneCUETP8M1	35.6
ST_t-channel_4f_leptonDecays_13TeV-amcatnlo-pythia8_TuneCUETP8M1	70.3144
ST_t-channel_antitop_4f_leptonDecays_13TeV-powheg-pythia8_TuneCUETP8M1	26.2278
ST_s-channel_4f_leptonDecays_13TeV-amcatnlo-pythia8_TuneCUETP8M1	3.68064
WWTo2L2Nu_13TeV-powheg	10.481

Table 4.3: List of background samples used in this analysis (CMSSW 80X). In the first section of the table are listed the samples of the processes for which we use the simulation to extract the final yields and shapes, in the second section the samples of the processes we will estimate from data. The MC simulation is used to design the data driven methods and derive the associated systematics.

Sample	σ [pb]
ttWJets_13TeV_madgraphMLM	0.6105
ttZJets_13TeV_madgraphMLM	0.5297/0.692

Table 4.4: Leading-order $t\bar{t}W$ and $t\bar{t}Z$ samples used in the signal BDT training.

1035 using POWHEG interfaced to PYTHIA, or bare PYTHIA (see table 4.3 and [63]
1036 for more details).

Three lepton and Four lepton
HLT_DiMu9_Ele9_CaloIdL_TrackIdL_v*
HLT_Mu8_DiEle12_CaloIdL_TrackIdL_v*
HLT_TripleMu_12_10_5_v*
HLT_Ele16_Ele12_Ele8_CaloIdL_TrackIdL_v*
HLT_Mu23_TrkIsoVVL_Ele8_CaloIdL_TrackIdL_IsoVL_v*
HLT_Mu23_TrkIsoVVL_Ele8_CaloIdL_TrackIdL_IsoVL_DZ_v*
HLT_Mu8_TrkIsoVVL_Ele23_CaloIdL_TrackIdL_IsoVL_v*
HLT_Mu8_TrkIsoVVL_Ele23_CaloIdL_TrackIdL_IsoVL_DZ_v*
HLT_Ele23_Ele12_CaloIdL_TrackIdL_IsoVL_DZ_v*
HLT_Mu17_TrkIsoVVL_Mu8_TrkIsoVVL_DZ_v*
HLT_Mu17_TrkIsoVVL_TkMu8_TrkIsoVVL_DZ_v*
HLT_IsoMu22_v*
HLT_IsoTkMu22_v*
HLT_IsoMu22_eta2p1_v*
HLT_IsoTkMu22_eta2p1_v*
HLT_IsoMu24_v*
HLT_IsoTkMu24_v*
HLT_Ele27_WPTight_Gsf_v*
HLT_Ele25_eta2p1_WPTight_Gsf_v*
HLT_Ele27_eta2p1_WPLoose_Gsf_v*

Table 4.5: Table of high-level triggers that we consider in the analysis.

1037 4.2.2 Triggers

1038 We consider online-reconstructed events triggered by one, two, or three leptons.
 1039 Single-lepton triggers are included to boost the acceptance of events where the p_T of
 1040 the sub-leading lepton falls below the threshold of the double-lepton triggers. Ad-
 1041 ditionally, by including double-lepton triggers in the ≥ 3 lepton category, as well
 1042 as single-lepton triggers in all categories, we increase the efficiency, considering the
 1043 logical “or” of the trigger decisions of all the individual triggers in a given category.
 1044 Tab. 4.5 shows the lowest-threshold non-prescaled triggers present in the High-Level
 1045 Trigger (HLT) menus for both Monte-Carlo and data in 2016.

1046 4.2.2.1 Trigger efficiency scale factors

1047 The efficiency of events to pass the trigger is measured in simulation (trivially using
 1048 generator information) and in the data (using event collected by an uncorrelated

Category	Scale Factor
ee	1.01 ± 0.02
e μ	1.01 ± 0.01
$\mu\mu$	1.00 ± 0.01
3l	1.00 ± 0.03

Table 4.6: Trigger efficiency scale factors and associated uncertainties, shown here rounded to the nearest percent.

1049 MET trigger). Small differences between the data and MC efficiencies are corrected
 1050 by applying scale factors as shown in Tab. 4.6. The exact procedure and control plots
 1051 are documented in [66] for the current analysis.

1052 4.3 Object Identification and event selection

1053 4.3.1 Jets and b tagging

1054 The analysis uses anti- k_t (0.4) particle-flow (PF) jets, corrected for charged hadrons
 1055 not coming from the primary vertex (charged hadron subtraction), and having jet
 1056 energy corrections (`Summer16_23Sep2016V3`) applied as a function of the jet E_T and
 1057 η . Jets are only considered if they have a transverse energy above 25GeV.

1058 In addition, they are required to be separated from any lepton candidates passing
 1059 the fakeable object selections (see Tables 4.7 and 4.8) by $\Delta R > 0.4$.

1060 The loose and medium working points of the CSV b-tagging algorithm are used to
 1061 identify b jets. Data/simulation differences in the b tagging performance are corrected
 1062 by applying per-jet weights to the simulation, dependent on the jet p_T , eta, b tagging
 1063 discriminator, and flavor (from simulation truth) [67]. The per-event weight is taken
 1064 as the product of the per-jet weights, including those of the jets associated to the
 1065 leptons. More details can be found in the corresponding $t\bar{t}H$ documentation [63, 66].

1066 **4.3.2 Lepton selection**

Cut	Loose	Fakeable object	Tight
$ \eta < 2.4$	✓	✓	✓
p_T	$> 5\text{GeV}$	$> 15\text{GeV}$	$> 15\text{GeV}$
$ d_{xy} < 0.05 \text{ (cm)}$	✓	✓	✓
$ d_z < 0.1 \text{ (cm)}$	✓	✓	✓
$\text{SIP}_{3D} < 8$	✓	✓	✓
$I_{\text{mini}} < 0.4$	✓	✓	✓
is Loose Muon	✓	✓	✓
jet CSV	—	< 0.8484	< 0.8484
is Medium Muon	—	—	✓
tight-charge	—	—	✓
lepMVA > 0.90	—	—	✓

Table 4.7: Requirements on each of the three muon selections. In the cases where the cut values change between the selections, those values are listed in the table. Otherwise, whether the cut is applied is indicated. For the two p_T^{ratio} and CSV rows, the cuts marked with a † are applied to leptons that fail the lepton MVA cut, while the loose cut value is applied to those that pass the lepton MVA cut.

1067 The lepton reconstruction and selection is identical to that used in the $t\bar{t}H$ mul-
 1068 tilepton analysis, as documented in Refs. [63, 66]. For details on the reconstruction
 1069 algorithms, isolation, pileup mitigation, and a description of the lepton MVA discrim-
 1070 inator and validation plots thereof, we refer to that document since they are out of
 1071 the scope of this thesis. Three different selections are defined both for the electron
 1072 and muon object identification: the *Loose*, *Fakeable Object*, and *Tight* selection. As
 1073 described in more detail later, these are used for event level vetoes, the fake rate
 1074 estimation application region, and the final signal selection, respectively. The p_T of
 1075 fakeable objects is defined as $0.85 \times p_T(\text{jet})$, where the jet is the one associated to the
 1076 lepton object. This mitigates the dependence of the fake rate on the momentum of
 1077 the fakeable object and thereby improves the precision of the method.

1078 Tables 4.7 and 4.8 list the full criteria for the different selections of muons and
 1079 electrons.

Cut	Loose	Fakeable Object	Tight
$ \eta < 2.5$	✓	✓	✓
p_T	$> 7\text{GeV}$	$> 15\text{GeV}$	$> 15\text{GeV}$
$ d_{xy} < 0.05 \text{ (cm)}$	✓	✓	✓
$ d_z < 0.1 \text{ (cm)}$	✓	✓	✓
$\text{SIP}_{3D} < 8$	✓	✓	✓
$I_{\text{mini}} < 0.4$	✓	✓	✓
MVA ID $> (0.0, 0.0, 0.7)$	✓	✓	✓
$\sigma_{i\eta i\eta} < (0.011, 0.011, 0.030)$	—	✓	✓
$\text{H/E} < (0.10, 0.10, 0.07)$	—	✓	✓
$\Delta\eta_{in} < (0.01, 0.01, 0.008)$	—	✓	✓
$\Delta\phi_{in} < (0.04, 0.04, 0.07)$	—	✓	✓
$-0.05 < 1/E - 1/p < (0.010, 0.010, 0.005)$	—	✓	✓
p_T^{ratio}	—	$> 0.5 \dagger / -$	—
jet CSV	—	$< 0.3 \dagger / < 0.8484$	< 0.8484
tight-charge	—	—	✓
conversion rejection	—	—	✓
Number of missing hits	< 2	$== 0$	$== 0$
lepMVA > 0.90	—	—	✓

Table 4.8: Criteria for each of the three electron selections. In cases where the cut values change between selections, those values are listed in the table. Otherwise, whether the cut is applied is indicated. In some cases, the cut values change for different η ranges. These ranges are $0 < |\eta| < 0.8$, $0.8 < |\eta| < 1.479$, and $1.479 < |\eta| < 2.5$ and the respective cut values are given in the form (value₁, value₂, value₃).

4.3.3 Lepton selection efficiency

Efficiencies of reconstruction and selecting loose leptons are measured both for muons and electrons using a tag and probe method on both data and MC, using $Z \rightarrow \ell^+\ell^-$. Corresponding scale factors are derived from the ratio of efficiencies and applied to the selected These. Events are produced for the leptonic SUSY analyses using equivalent lepton selections and recycled for the $t\bar{t}H$ analysis as well as for this analysis. The efficiencies of applying the tight selection as defined in Tables 4.7 and 4.8, on the loose leptons are determined again by using a tag and probe method on a sample of DY-enriched events. They are documented for the $t\bar{t}H$ analysis in Ref. [66] and are exactly equivalent for this analysis.

1090 4.4 Background predictions

1091 The modeling of reducible and irreducible backgrounds in this analysis uses the exact
 1092 methods, analysis code, and ROOT trees used for the $t\bar{t}H$ multilepton analysis. We
 1093 give a brief description of the methods and refer to the documentation of that analysis
 1094 in Refs. [63, 66] for any details.

1095 The backgrounds in three-lepton final states can be split in two broad categories:
 1096 irreducible backgrounds with genuine prompt leptons (i.e. from on-shell W and Z
 1097 boson decays); and reducible backgrounds where at least one of the leptons is “non-
 1098 prompt”, i.e. produced within a hadronic jet, either a genuine lepton from heavy
 1099 flavor decays, or simply mis-reconstructed jets.

1100 Irreducible backgrounds can be reliably estimated directly from Monte-Carlo sim-
 1101 ulated events, using higher-order cross sections or data control regions for the overall
 1102 normalization. This is done in this analysis for all backgrounds involving prompt lep-
 1103 tons: $t\bar{t}W$, $t\bar{t}Z$, $t\bar{t}H$, WZ , ZZ , $W^\pm W^\pm qq$, $t\bar{t}t\bar{t}$, tZq , tZW , WWW , WWZ , WZZ ,
 1104 ZZZ .

1105 Reducible backgrounds, on the other hand, are not well predicted by simulation,
 1106 and are estimated using data-driven methods. In the case of non-prompt leptons, a
 1107 fake rate method is used, where the contribution to the final selection is estimated by
 1108 extrapolating from a sideband (or “application region”) with a looser lepton definition
 1109 (the fakeable object definitions in Tabs. 4.7 and 4.8) to the signal selection. The tight-
 1110 to-loose ratios (or “fake rates”) are measured in several background dominated data
 1111 events with dedicated triggers, subtracting the residual prompt lepton contribution
 1112 using MC. Non-prompt leptons in our signal regions are predominantly produced in $t\bar{t}$
 1113 events, with a much smaller contribution, from Drell–Yan production. The systematic
 1114 uncertainty on the normalization of the non-prompt background estimation is on the

order of 50%, and thereby one of the dominant limitations on the performance of multilepton analyses in general and this analysis in particular. It consists of several individual sources, such as the result of closure tests of the method using simulated events, limited statistics in the data control regions due to necessary prescaling of lepton triggers, and the uncertainty in the subtraction of residual prompt leptons from the control region.

The fake background where the leptons pass the looser selection are weighted according to how many of them fail the tight criteria. Events with a single failing lepton are weighted with the factor $f/(1-f)$ for the estimate to the tight selection region, where f is the fake rate. Events with two failing leptons are given the negative weight $-f_i f_j / (1-f_i)(1-f_j)$, and for three leptons the weight is positive and equal to the product of $f/(1-f)$ factor evaluated for each failing lepton.

Figures 4.2 show the distributions of some relevant kinematic variables, normalized to the cross section of the respective processes and to the integrated luminosity.

4.5 Signal discrimination

The tHq signal is separated from the main backgrounds using a boosted decision tree (BDT) classifier, trained on simulated signal and background events. A set of discriminating variables are given as input to the BDT which produces a output distribution maximizing the discrimination power. Table 4.9 lists the input variables used while Figures 4.3 show their distributions for the relevant signal and background samples, for the three lepton channel. Two BDT classifiers are trained for the two main backgrounds expected in the analysis: events with prompt leptons from $t\bar{t}W$ and $t\bar{t}Z$ (also referred to as $t\bar{t}V$), and events with non-prompt leptons from $t\bar{t}$. The datasets used in the training are the tHq signal (see Tab. 4.1), and LO MADGRAPH samples

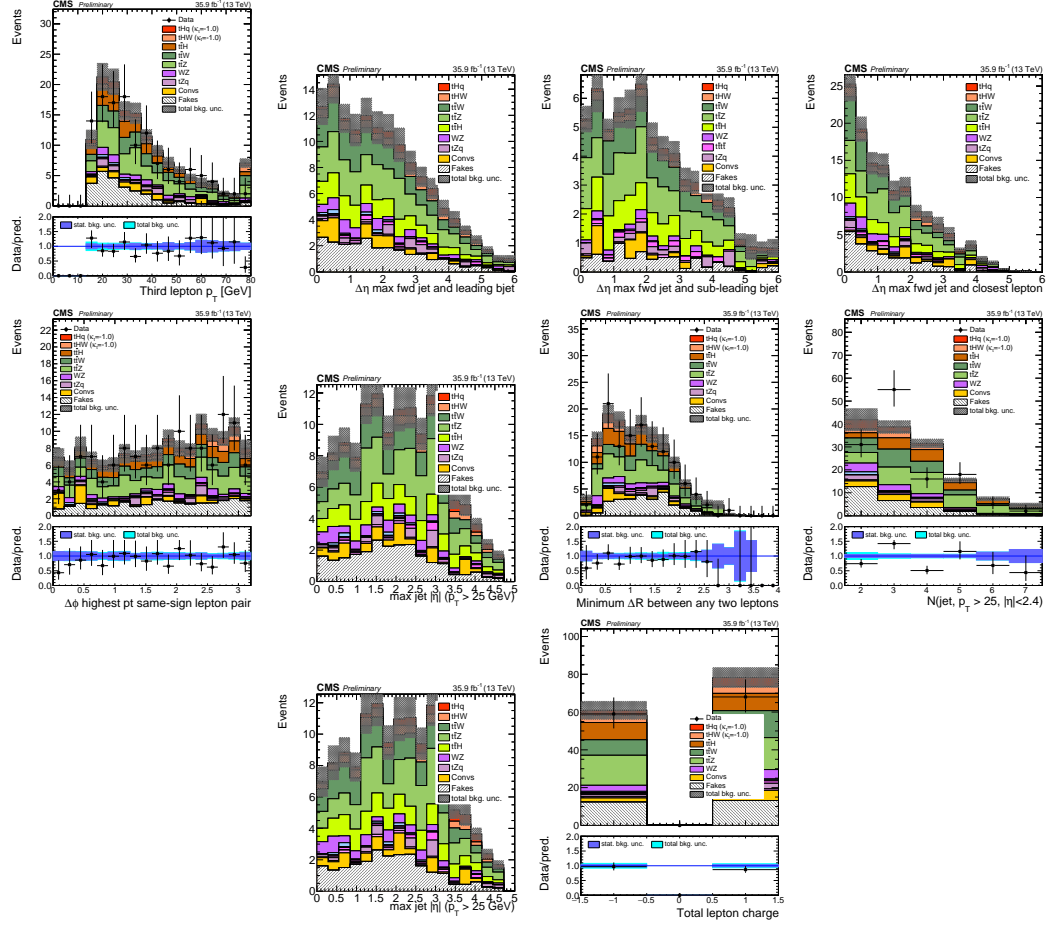


Figure 4.2: Distributions of input variables to the BDT for signal discrimination, three lepton channel, normalized to their cross section and to 35.9fb^{-1} .

of $t\bar{t}W$ and $t\bar{t}Z$, in an admixture proportional to their respective cross sections (see Tab. 4.4).

The MVA analysis consist of two stages: first a “training” where the MVA method is trained to discriminate between simulated signal and background events, then a “test” stage where the trained algorithm is used to classify different events from the samples. The sample is obtained from a pre-selection (see Tab. ?? with pre-selection cuts). Figures 4.4 show the input variables distributions as seen by the MVA algorithm. Note that in contrast to the distributions in Fig. 4.3 only the main backgrounds ($t\bar{t}$ from simulation, $t\bar{t}V$) are included.

Variable name	Description
nJet25	Number of jets with $p_T > 25$ GeV, $ \eta < 2.4$
MaxEtaJet25	Maximum $ \eta $ of any (non-CSV-loose) jet with $p_T > 25$ GeV
totCharge	Sum of lepton charges
nJetEta1	Number of jets with $ \eta > 1.0$, non-CSV-loose
detaFwdJetBJet	$\Delta\eta$ between forward light jet and hardest CSV loose jet
detaFwdJet2BJet	$\Delta\eta$ between forward light jet and second hardest CSV loose jet (defaults to -1 in events with only one CSV loose jet)
detaFwdJetClosestLep	$\Delta\eta$ between forward light jet and closest lepton
dphiHighestPtSSPair	$\Delta\phi$ of highest p_T same-sign lepton pair
minDRll	minimum ΔR between any two leptons
Lep3Pt/Lep2Pt	p_T of the 3 rd lepton (2 nd for ss2l)

Table 4.9: MVA input discriminating variables

1148 Note that splitting the training in two groups reveals that some variables show
 1149 opposite behavior for the two background sources; potentially screening the discrimi-
 1150 nation power if they were to be used in a single discriminant. For some other variables
 1151 the distributions are similar in both background cases.

1152 From table 4.9, it is clear that the input variables are correlated to some extend.
 1153 These correlations play an important role for some MVA methods like the Fisher
 1154 discriminant method in which the first step consist of performing a linear transfor-
 1155 mation to an phase space where the correlations between variables are removed. In
 1156 case a boosted decision tree (BDT) method however, correlations do not affect the
 1157 performance. Figure 4.6 show the linear correlation coefficients for signal and back-
 1158 ground for the two training cases (the signal values are identical by construction). As
 1159 expected, strong correlations appears for variables related to the forward jet activity.
 1160 Same trend is seen in case of the same sign dilepton channel in Figure ??.

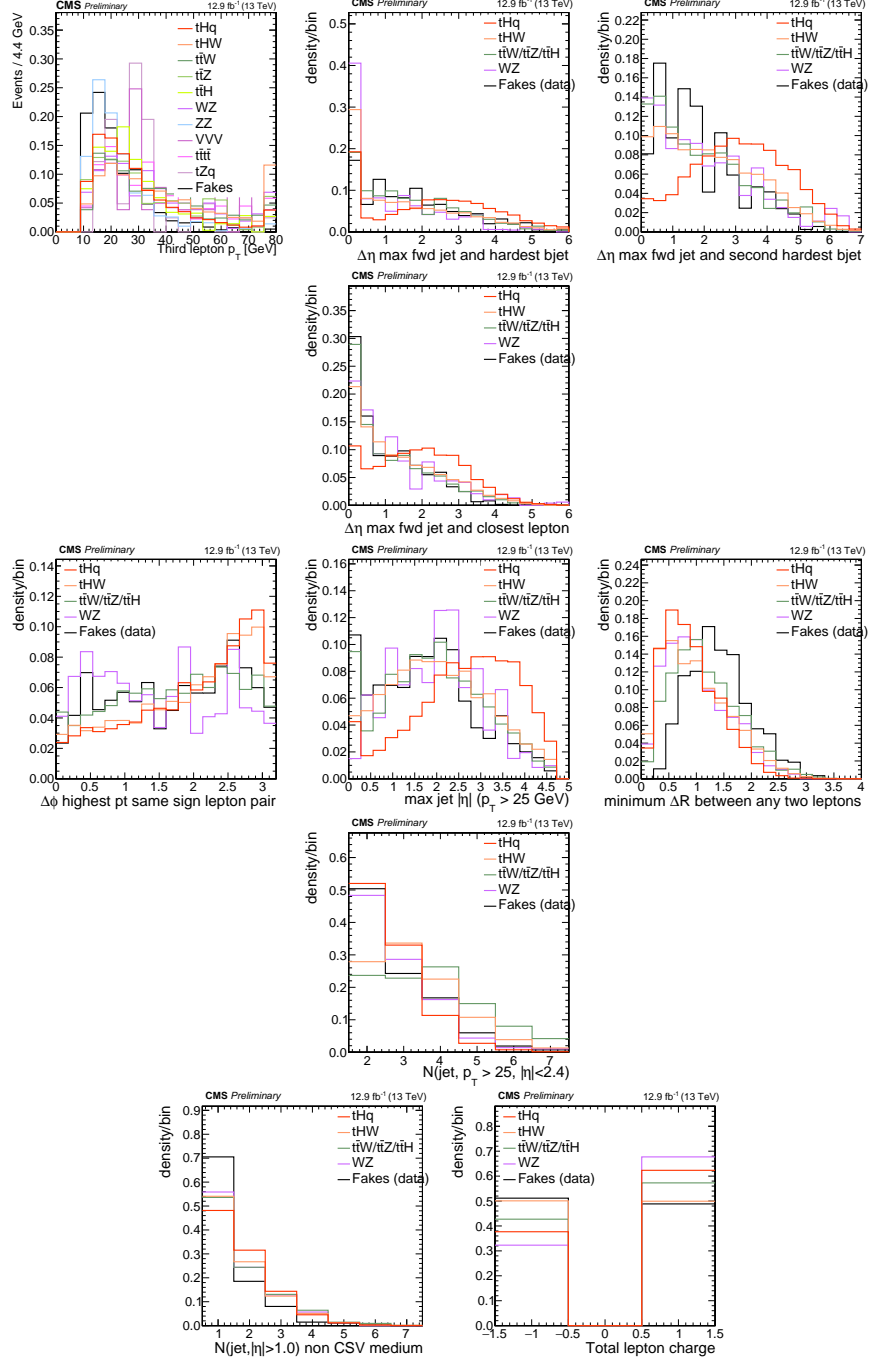


Figure 4.3: Distributions of input variables to the BDT for signal discrimination, three lepton channel.

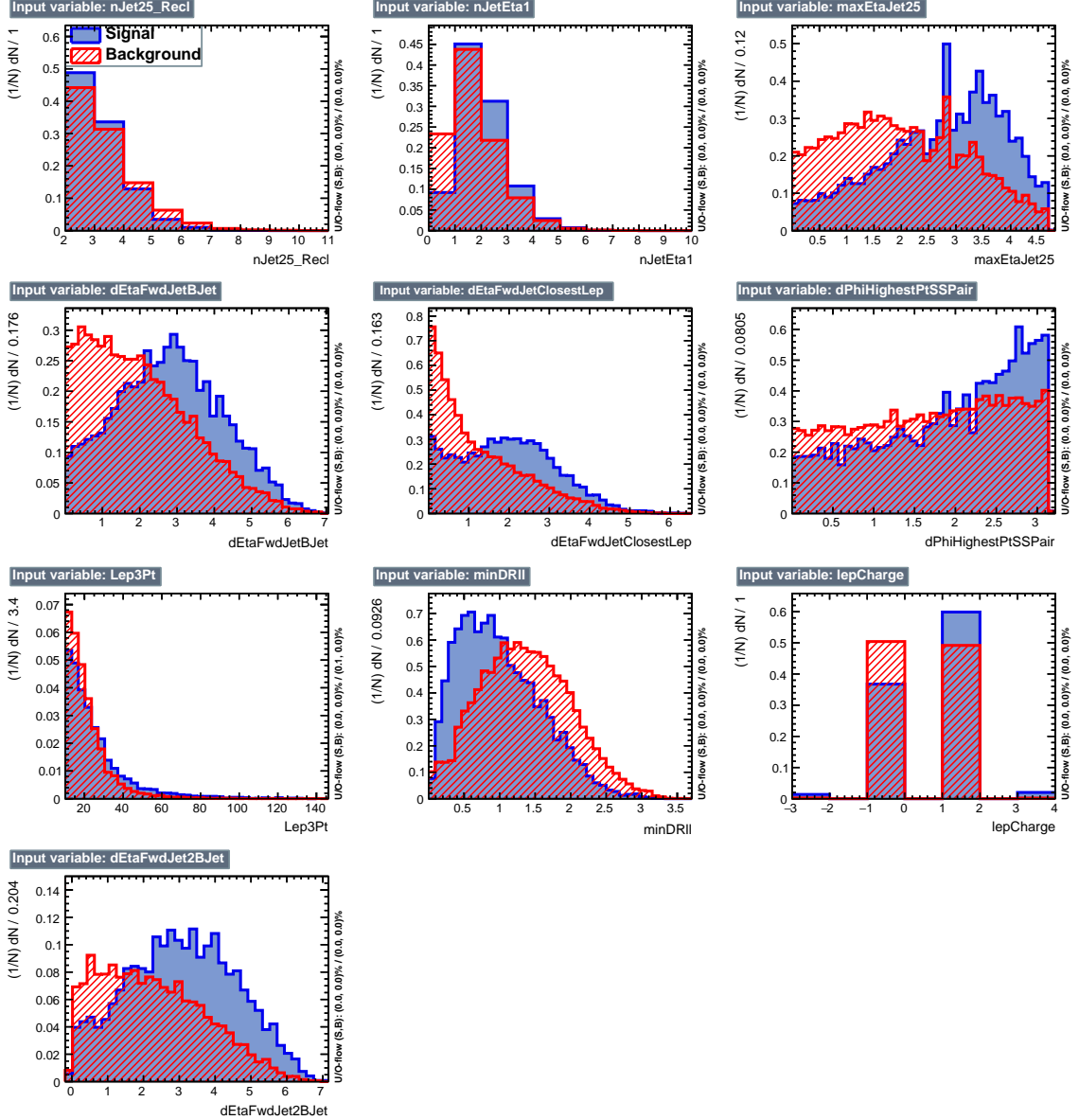


Figure 4.4: BDT inputs as seen by TMVA (signal, in blue, is tHq , background, in red, is $t\bar{t}$) for the three lepton channel, discriminated against $t\bar{t}$ (fakes) background.

1161 4.5.1 Classifiers response

1162 Several MVA algorithms were evaluated to determine the most appropriate method
 1163 for this analysis. The plots in Fig. 4.7 (top) show the background rejection as a
 1164 function of the signal efficiency for $t\bar{t}$ and $t\bar{t}V$ trainings (ROC curves) for the different

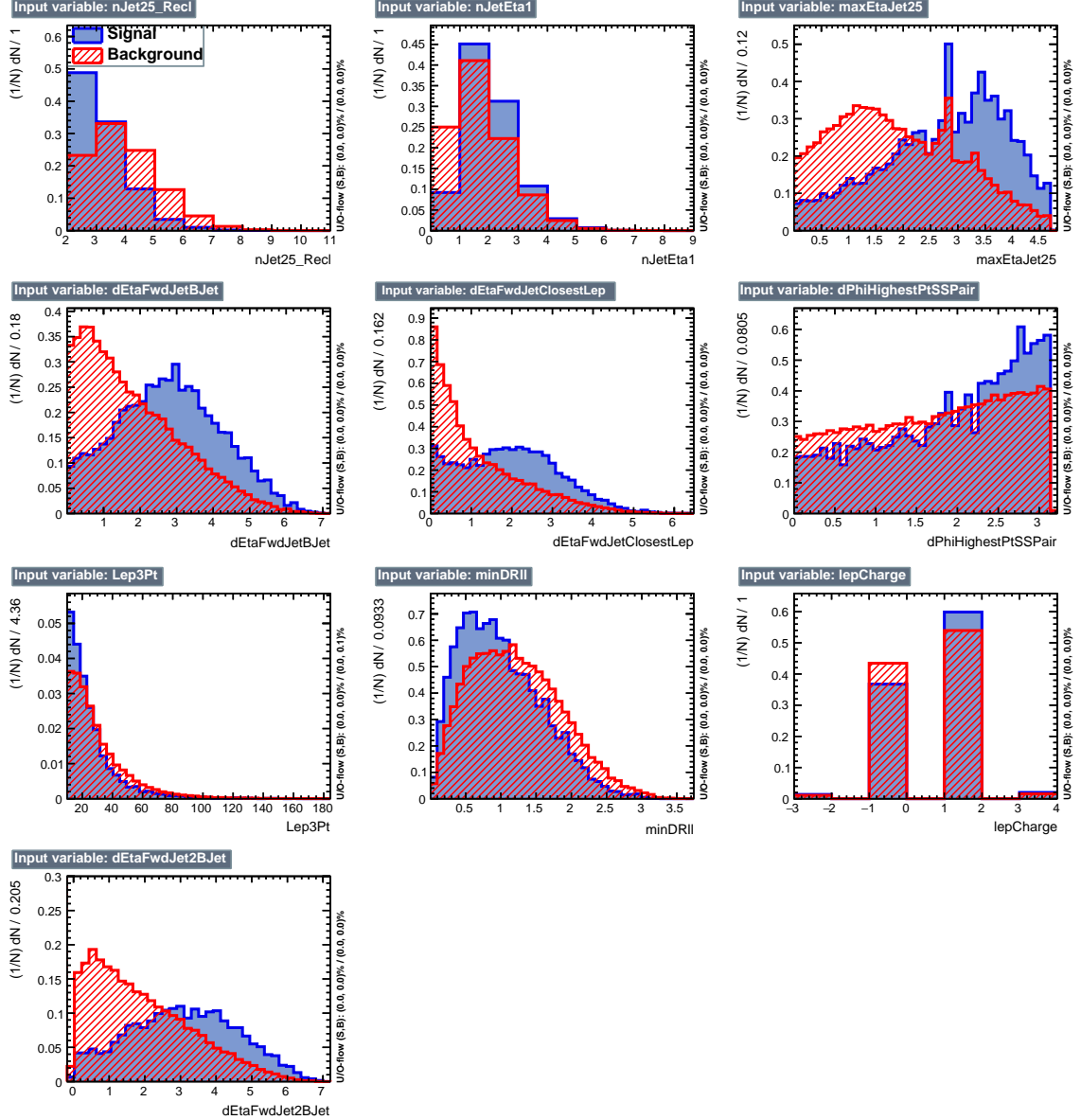


Figure 4.5: BDT inputs as seen by TMVA (signal, in blue, is tHq , background, in red, is $t\bar{t}W+t\bar{t}Z$) for the three lepton channel, discriminated against $t\bar{t}V$ background.

algorithms that were evaluated.

In both cases the gradient boosted decision tree (“BDTA_GRAD”) classifier offers the best results, followed by an adaptive BDT classifier (“BDTA”). The BDTA_GRAD classifier output distributions for signal and backgrounds are shown on the bottom of Fig. 4.7. As expected, a good discrimination power is obtained using default discrim-

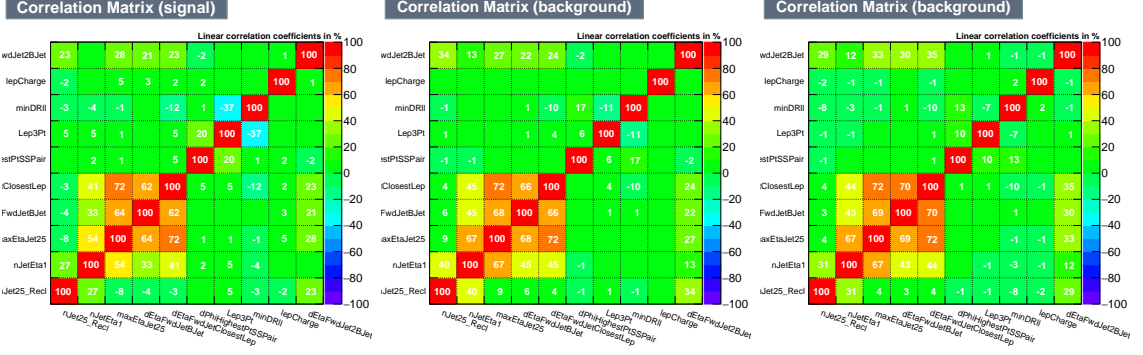


Figure 4.6: Signal (left), $t\bar{t}$ background (middle), and $t\bar{t}V$ background (right.) correlation matrices for the input variables in the TMVA analysis for the three lepton channel.

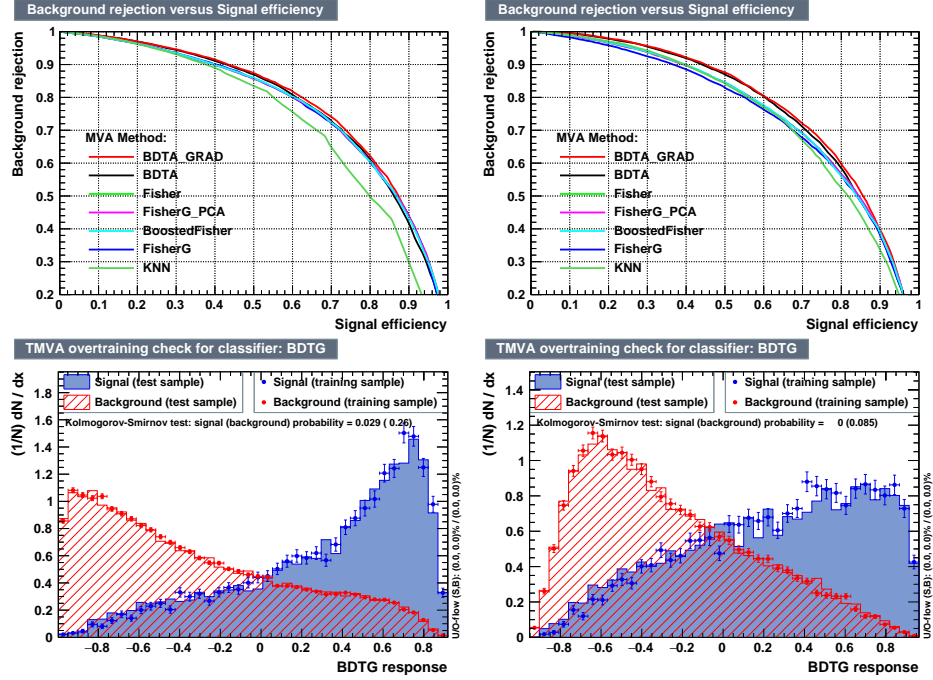


Figure 4.7: Top: background rejection vs signal efficiency (ROC curves) for various MVA classifiers (top) in the three lepton channel against $t\bar{t}V$ (left) and $t\bar{t}$ (right). Bottom: classifier output distributions for the gradient boosted decision trees, for training against $t\bar{t}V$ (left) and against $t\bar{t}$ (right).

inator parameter values, with minimal overtraining. TMVA provides a ranking of the
1170 input variables by their importance in the classification process, shown in Tab. 4.10.
1171
The TMVA settings used in the BDT training are shown in Tab. 4.11.
1172

ttbar training			ttV training		
Rank	Variable	Importance	Variable	Importance	Importance
1	minDRll	1.329e-01	dEtaFwdJetBJet	1.264e-01	
2	dEtaFwdJetClosestLep	1.294e-01	Lep3Pt	1.224e-01	
3	dEtaFwdJetBJet	1.209e-01	maxEtaJet25	1.221e-01	
4	dPhiHighestPtSSPair	1.192e-01	dEtaFwdJet2BJet	1.204e-01	
5	Lep3Pt	1.158e-01	dEtaFwdJetClosestLep	1.177e-01	
6	maxEtaJet25	1.121e-01	minDRll	1.143e-01	
7	dEtaFwdJet2BJet	9.363e-02	dPhiHighestPtSSPair	9.777e-02	
8	nJetEta1	6.730e-02	nJet25_Recl	9.034e-02	
9	nJet25_Recl	6.178e-02	nJetEta1	4.749e-02	
10	lepCharge	4.701e-02	lepCharge	4.116e-02	

Table 4.10: TMVA input variables ranking for BDTA_GRAD method for the trainings in the three lepton channel. For both trainings the rankings show almost the same 5 variables in the first places.

```
TMVA.Types.kBDT
NTrees=800
BoostType=Grad
Shrinkage=0.10
!UseBaggedGrad
nCuts=50
MaxDepth=3
NegWeightTreatment=PairNegWeightsGlobal
CreateMVAPdfs
```

Table 4.11: TMVA configuration used in the BDT training.

1173 4.6 Additional discriminating variables

1174 Two additional discriminating variables were tested considering the fact that the
 1175 forward jet in the background could come from the pileup; since we have a real
 1176 forward jet in the signal, it could give some improvement in the discriminating power.
 1177 The additional variables describe the forward jet momentum (fwdJetPt25) and the
 1178 forward jet identification(fwdJetPUID). Distributions for these variables in the three
 1179 lepton channel are shown in the figure 4.8. The forward jet identification distribution
 1180 show that for both, signal and background, jets are mostly real jets.

1181 The testing was made including in the MVA input one variable at a time, so we

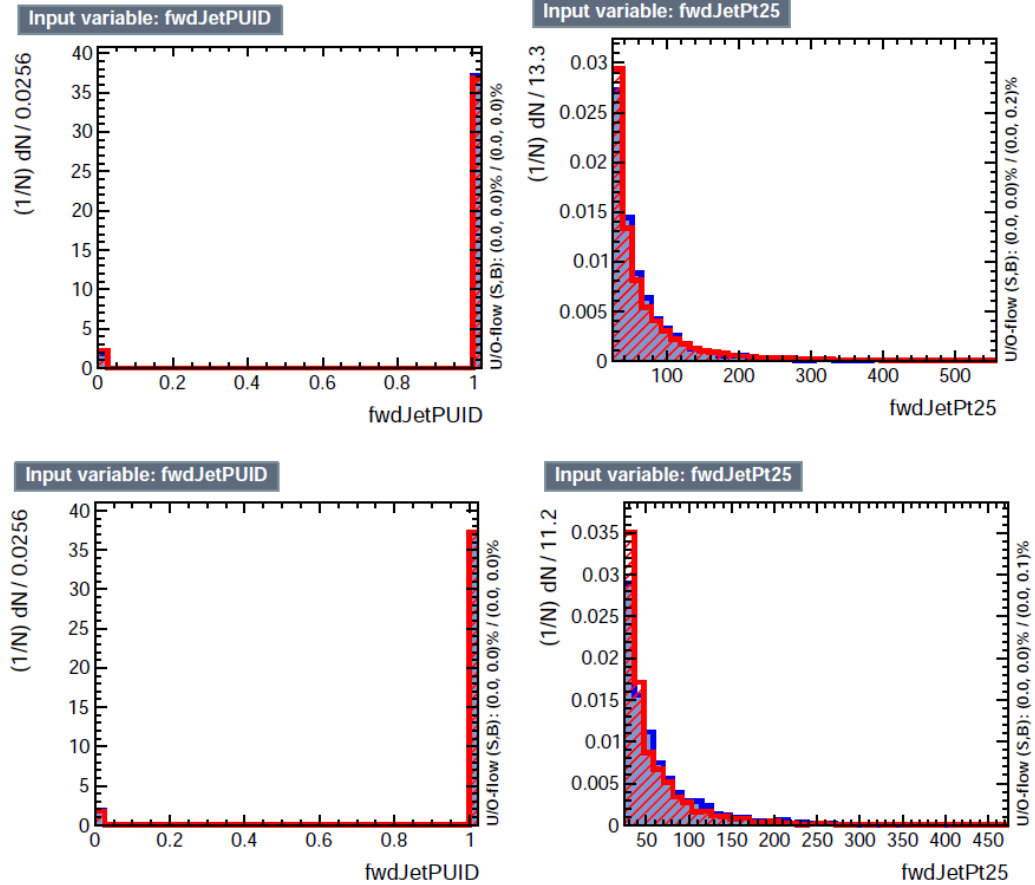


Figure 4.8: Additional discriminating variables distributions for ttV training (Top row) and tt training (bottom row) in the three lepton channel. The origin of the jets in the forward jet identification distribution is tagged as 0 for “pileup jets” while “real jets” are tagged as 1.

1182 can evaluate the discrimination power of each variable, and then both simultaneously.
 1183 fwdJetPUID was ranked in the last place in importance (11) in both training (ttV
 1184 and tt) while fwdJetPt25 was ranked 3 in the ttV training and 7 in the tt training.
 1185 When training using 12 variables, fwdJetPt25 was ranked 5 and 7 in the ttV and tt
 1186 trainings respectively, while fwdJetPUID was ranked 12 in both cases.

1187 The improvement in the discrimination performance provided by the additional
 1188 variables is about 1%, so it was decided not to include them in the procedure. Table
 1189 4.12 show the ROC-integral for all the testing cases we made.

ROC-integral	
base 10 var ttv	0.848
+ fwdJetPUID ttv	0.849
+ fwdJetPt25 ttv	0.856
12 var ttv	0.856
<hr/>	
base 10 var tt	0.777
+ fwdJetPUID tt	0.777
+ fwdJetPt25 tt	0.787
12 var	0.787

Table 4.12: ROC-integral for all the testing cases we made in the evaluation of the additional variables discriminating power. The improvement in the discrimination performance provided by the additional variables is about 1%

₁₁₉₀ **Chapter 5**

₁₁₉₁ **The CMS forward pixel detector**

₁₁₉₂ **5.0.1 The phase 1 FPix upgrade**

₁₁₉₃ **5.0.2 FPix module production line**

₁₁₉₄ **5.0.3 The Gluing stage**

₁₁₉₅ **5.0.4 The Encapsulation stage**

₁₁₉₆ **5.0.5 The FPix module production yields**

¹¹⁹⁷ References

- ¹¹⁹⁸ [1] D.J. Griffiths, “Introduction to electrodynamics”. 4th ed. Pearson, (2013).
- ¹¹⁹⁹ [2] F. Mandl, G. Shaw. “Quantum field theory.” Chichester: Wiley (2009).
- ¹²⁰⁰ [3] F. Halzen, and A.D. Martin, “Quarks and leptons: An introductory course in
¹²⁰¹ modern particle physics”. New York: Wiley, (1984) .
- ¹²⁰² [4] J.C. Maxwell. “A dynamical theory of the electromagnetic field”. Philosophical Transactions of the Royal Society of London. 155: 459–512.(1865)
¹²⁰³
¹²⁰⁴ doi:10.1098/rstl.1865.0008
- ¹²⁰⁵ [5] M. Planck. “Über das Gesetz der Energieverteilung im Normalspektrum”.
¹²⁰⁶ Annalen der Physik. 4 (3): 553.(1901).
- ¹²⁰⁷ [6] A. Einstein “Über einen die Erzeugung und Verwandlung des Lichtes betref-
¹²⁰⁸ fenden heuristischen Gesichtspunkt”. Annalen der Physik. 17 (6): 132–148,
¹²⁰⁹ (1905).
- ¹²¹⁰ [7] A. Einstein. “Über die von der molekularkinetischen Theorie der Wärme
¹²¹¹ geforderte Bewegung von in ruhenden Flüssigkeiten suspendierten Teilchen”.
¹²¹² Annalen der Physik. 17 (8): 549–560, (1905).
- ¹²¹³ [8] A. Einstein. “Zur Elektrodynamik bewegter Körper”. Annalen der Physik. 17
¹²¹⁴ (10): 891–921, (1905).

- 1215 [9] A. Einstein, "Ist die TrÄdgheit eines KÃürpers von seinem Energieinhalt ab-
 1216 hÃdngig?". Annalen der Physik. 18 (13): 639â€¢641, (1905).
- 1217 [10] B. P. Abbott et al. "Observation of Gravitational Waves from a Binary Black
 1218 Hole Merger". PRL 116, 061102 (2016).
- 1219 [11] J. Schwinger. "Quantum Electrodynamics. I. A Covariant Formulation". Phys-
 1220 ical Review. 74 (10): 1439â€¢61, (1948).
- 1221 [12] R. P. Feynman. "Spaceâ€¢Time Approach to Quantum Electrodynamics".
 1222 Physical Review. 76 (6): 769â€¢89, (1949).
- 1223 [13] S. Tomonaga. "On a Relativistically Invariant Formulation of the Quantum
 1224 Theory of Wave Fields". Progress of Theoretical Physics. 1 (2): 27â€¢42, (1946).
- 1225 [14] S.L. Glashow. "Partial symmetries of weak interactions", Nucl. Phys. 22 579-
 1226 588, (1961).
- 1227 [15] A. Salam, J.C. Ward. "Electromagnetic and weak interactions", Physics Letters
 1228 13 168-171, (1964).
- 1229 [16] S. Weinberg, "A model of leptons", Physical Review Letters, vol. 19, no. 21, p.
 1230 1264, (1967).
- 1231 [17] E. Noether, "Invariante Variationsprobleme", Nachrichten von der Gesellschaft
 1232 der Wissenschaften zu GÃüttingen, mathematisch-physikalische Klasse, vol.
 1233 1918, pp. 235â€¢257, (1918).
- 1234 [18] File:Standard_Model_of_Elementary_Particle_dark.svg. (2017, June 12)
 1235 Wikimedia Commons, the free media repository. Retrieved November 27,
 1236 2017 from <https://www.collegiate-advanced-electricity.com/single-post/2017/04/10/The-Standard-Model-of-Particle-Physics>.

- 1238 [19] M. Goldhaber, L. Grodzins, A.W. Sunyar “Helicity of Neutrinos”, Phys. Rev.
 1239 109, 1015 (1958).
- 1240 [20] Palanque-Delabrouille N et al. “Neutrino masses and cosmology with Lyman-
 1241 alpha forest power spectrum”, JCAP 11 011 (2015).
- 1242 [21] C. Patrignani et al. (Particle Data Group), Chin. Phys. C, 40, 100001 (2016)
 1243 and 2017 update.
- 1244 [22] M. Gell-Mann. “A Schematic Model of Baryons and Mesons”. Physics Letters.
 1245 8 (3): 214–215 (1964).
- 1246 [23] G. Zweig. “An SU(3) Model for Strong Interaction Symmetry and its Breaking”
 1247 (PDF). CERN Report No.8182/TH.401 (1964).
- 1248 [24] G. Zweig. “An SU(3) Model for Strong Interaction Symmetry and its Breaking:
 1249 II” (PDF). CERN Report No.8419/TH.412(1964).
- 1250 [25] M. Gell-Mann. “The Interpretation of the New Particles as Displaced Charged
 1251 Multiplets”. Il Nuovo Cimento 4: 848. (1956).
- 1252 [26] T. Nakano, K. Nishijima. “Charge Independence for V-particles”. Progress of
 1253 Theoretical Physics 10 (5): 581-582. (1953).
- 1254 [27] N. Cabibbo, “Unitary symmetry and leptonic decays” Physical Review Letters,
 1255 vol. 10, no. 12, p. 531, (1963).
- 1256 [28] M.Kobayashi, T.Maskawa, “CP-violation in the renormalizable theory of weak
 1257 interaction,” Progress of Theoretical Physics, vol. 49, no. 2, pp. 652-657, (1973).
- 1258 [29] File:Weak Decay (flipped).svg. (2017, June 12). Wikimedia Com-
 1259 mons, the free media repository. Retrieved November 27, 2017

- 1260 from `https : //commons.wikimedia.org/w/index.php?title = File :`
 1261 `Weak_Decay_(flipped).svg&oldid = 247498592.`
- 1262 [30] Georgia Tech University. Coupling Constants for the Fundamental
 1263 Forces(2005). Retrieved January 10, 2018, from `http://hyperphysics.phy –`
 1264 `astr.gsu.edu/hbase/Forces/couple.html#c2`
- 1265 [31] M. Strassler. (May 31, 2013).The Strengths of the Known Forces. Retrieved
 1266 January 10, 2018, from `https://profmattstrassler.com/articles – and –`
 1267 `posts/particle – physics – basics/the – known – forces – of – nature/the –`
 1268 `strength – of – the – known – forces/`
- 1269 [32] M. Peskin, D. Schroeder, “An introduction to quantum field theory”. Perseus
 1270 Books Publishing L.L.C., (1995).
- 1271 [33] A. Pich. “The Standard Model of Electroweak Interactions”
 1272 `https://arxiv.org/abs/1201.0537`
- 1273 [34] F.Bellaiche. (2012, 2 September). “What’s this Higgs boson anyway?”. Retrieved
 1274 from: `https://www.quantum-bits.org/?p=233`
- 1275 [35] M. Endres et al. Nature 487, 454-458 (2012) doi:10.1038/nature11255
- 1276 [36] F. Englert, R. Brout. “Broken Symmetry and the Mass of Gauge Vec-
 1277 tor Mesons”. Physical Review Letters. 13 (9): 321–323.(1964) Bib-
 1278 code:1964PhRvL..13..321E. doi:10.1103/PhysRevLett.13.321
- 1279 [37] P.Higgs. “Broken Symmetries and the Masses of Gauge Bosons”. Physical
 1280 Review Letters. 13 (16): 508–509,(1964). Bibcode:1964PhRvL..13..508H.
 1281 doi:10.1103/PhysRevLett.13.508.

- 1282 [38] G.Guralnik, C.R. Hagen and T.W.B. Kibble. “Global Conservation Laws and
 1283 Massless Particles”. Physical Review Letters. 13 (20): 585–587, (1964). Bib-
 1284 code:1964PhRvL..13..585G. doi:10.1103/PhysRevLett.13.585.
- 1285 [39] CMS collaboration. “Observation of a new boson at a mass of 125
 1286 GeV with the CMS experiment at the LHC”. Physics Letters B.
 1287 716 (1): 30–61 (2012). arXiv:1207.7235. Bibcode:2012PhLB..716...30C.
 1288 doi:10.1016/j.physletb.2012.08.021
- 1289 [40] ATLAS collaboration. “Observation of a New Particle in the Search for the Stan-
 1290 dard Model Higgs Boson with the ATLAS Detector at the LHC”. Physics Let-
 1291 ters B. 716 (1): 1–29(2012). arXiv:1207.7214 Bibcode:2012PhLB..716....1A.
 1292 doi:10.1016/j.physletb.2012.08.020.
- 1293 [41] ATLAS collaboration; CMS collaboration (26 March 2015). “Combined
 1294 Measurement of the Higgs Boson Mass in pp Collisions at $\sqrt{s}=7$ and
 1295 8 TeV with the ATLAS and CMS Experiments”. Physical Review Let-
 1296 ters. 114 (19): 191803. arXiv:1503.07589. Bibcode:2015PhRvL.114s1803A.
 1297 doi:10.1103/PhysRevLett.114.191803.
- 1298 [42] CMS Collaboration, “SM Higgs Branching Ratios and To-
 1299 tal Decay Widths (up-date in CERN Report4 2016)”.
 1300 <https://twiki.cern.ch/twiki/bin/view/LHCPhysics/CERNYellowReportPageBR>, last accessed on 17.12.2017.
- 1302 [43] R.Grant V. “Determination of Higgs branching ratios in $H \rightarrow W^+W^- \rightarrow l^+l^- jj$ and $H \rightarrow ZZ \rightarrow l^+l^- jj$ channels”. Physics Department, Uni-
 1303 versity of Tennessee (Dated: October 31, 2012). Retrieved from
 1304 <http://aesop.phys.utk.edu/ph611/2012/projects/Riley.pdf>

- 1306 [44] LHC Higgs Cross Section Working Group, Denner, A., Heinemeyer, S. et al.
 1307 “Standard model Higgs-boson branching ratios with uncertainties”. Eur. Phys.
 1308 J. C (2011) 71: 1753. <https://doi.org/10.1140/epjc/s10052-011-1753-8>
- 1309 [45] LHC InternationalMasterclasses“When protons collide”. Retrieved from
 1310 http://atlas.physicsmasterclasses.org/en/zpath_protoncollisions.htm
- 1311 [46] F. Maltoni, K. Paul, T. Stelzer, and S. Willenbrock, “Associated production
 1312 of Higgs and single top at hadron colliders”, Phys.Rev. D64 (2001) 094023,
 1313 [hep-ph/0106293].
- 1314 [47] S. Biswas, E. Gabrielli, F. Margaroli, and B. Mele, “Direct constraints on the
 1315 top-Higgs coupling from the 8 TeV LHC data,” Journal of High Energy Physics,
 1316 vol. 07, p. 073, (2013).
- 1317 [48] M. Farina, C. Grojean, F. Maltoni, E. Salvioni, and A. Thamm, “Lifting de-
 1318 generacies in Higgs couplings using single top production in association with a
 1319 Higgs boson,” Journal of High Energy Physics, vol. 05, p. 022, (2013).
- 1320 [49] T.M. Tait and C.-P. Yuan, “Single top quark production as a window to physics
 1321 beyond the standard model”, Phys. Rev. D 63 (2000) 014018 [hep-ph/0007298].
- 1322 [50] F. Demartin, F. Maltoni, K. Mawatari, and M. Zaro, “Higgs production in
 1323 association with a single top quark at the LHC,” European Physical Journal C,
 1324 vol. 75, p. 267, (2015).
- 1325 [51] CMS Collaboration, “Modelling of the single top-quark pro-
 1326 duction in association with the Higgs boson at 13 TeV.”
 1327 <https://twiki.cern.ch/twiki/bin/viewauth/CMS/SingleTopHiggsGeneration13TeV>,
 1328 last accessed on 16.01.2018.

- 1329 [52] CMS Collaboration, “SM Higgs production cross sections at $\sqrt{s} = 13$ TeV.”
 1330 <https://twiki.cern.ch/twiki/bin/view/LHCPhysics/CERNYellowReportPageAt13TeV>,
 1331 last accessed on 16.01.2018.
- 1332 [53] S. Dawson, The effective W approximation, Nucl. Phys. B 249 (1985) 42.
- 1333 [54] S. Biswas, E. Gabrielli and B. Mele, JHEP 1301 (2013) 088 [arXiv:1211.0499
 1334 [hep-ph]].
- 1335 [55] F. Demartin, B. Maier, F. Maltoni, K. Mawatari, and M. Zaro, “tWH associated
 1336 production at the LHC”, European Physical Journal C, vol. 77, p. 34, (2017).
 1337 arXiv:1607.05862
- 1338 [56] LHC Higgs Cross Section Working Group, “Handbook of LHC Higgs Cross
 1339 Sections: 4.Deciphering the Nature of the Higgs Sector”, arXiv:1610.07922.
- 1340 [57] J. Ellis, D. S. Hwang, K. Sakurai, and M. Takeuchi.“Disentangling Higgs-Top
 1341 Couplings in Associated Production”, JHEP 1404 (2014) 004, [arXiv:1312.5736].
- 1342 [58] CMS Collaboration, V. Khachatryan et al., “Precise determination of the mass
 1343 of the Higgs boson and tests of compatibility of its couplings with the standard
 1344 model predictions using proton collisions at 7 and 8 TeV,” arXiv:1412.8662.
- 1345 [59] ATLAS Collaboration, G. Aad et al., “Updated coupling measurements of the
 1346 Higgs boson with the ATLAS detector using up to 25 fb^{-1} of proton-proton
 1347 collision data”, ATLAS-CONF-2014-009.
- 1348 [60] ATLAS and CMS Collaborations, “Measurements of the Higgs boson produc-
 1349 tion and decay rates and constraints on its couplings from a combined ATLAS
 1350 and CMS analysis of the LHC pp collision data at $\sqrt{s} = 7$ and 8 TeV,” (2016).
 1351 CERN-EP-2016-100, ATLAS-HIGG-2015-07, CMS-HIG-15-002.

- 1352 [61] CMS Collaboration, “Search for the associated production of a Higgs boson
 1353 with a single top quark in proton-proton collisions at $\sqrt{s} = 8$ TeV”, JHEP 06
 1354 (2016) 177,doi:10.1007/JHEP06(2016)177, arXiv:1509.08159.
- 1355 [62] B. Stieger, C. Jorda Lope et al., “Search for Associated Production of a Single
 1356 Top Quark and a Higgs Boson in Leptonic Channels”, CMS Analysis Note CMS
 1357 AN-14-140, 2014.
- 1358 [63] M. Peruzzi, C. Mueller, B. Stieger et al., “Search for ttH in multilepton final
 1359 states at $\sqrt{s} = 13$ TeV”, CMS Analysis Note CMS AN-16-211, 2016.
- 1360 [64] CMS Collaboration, “Search for H to bbar in association with a single top quark
 1361 as a test of Higgs boson couplings at $\sqrt{s} = 13$ TeV”, CMS Physics Analysis
 1362 Summary CMS-PAS-HIG-16-019, 2016.
- 1363 [65] B. Maier, “SingleTopHiggProduction13TeV”, February, 2016.
 1364 <https://twiki.cern.ch/twiki/bin/viewauth/CMS/SingleTopHiggsGeneration13TeV>.
- 1365 [66] M. Peruzzi, F. Romeo, B. Stieger et al., “Search for ttH in multilepton final1
 1366 states at $\sqrt{s} = 13$ TeV”, CMS Analysis Note CMS AN-17-029, 2017.
- 1367 [67] B. WG, “BtagRecommendation80XReReco”, February, 2017.
 1368 <https://twiki.cern.ch/twiki/bin/view/CMS/BtagRecommendation80XReReco>.